

**Studies on attaining $0.5(\text{Ba}_{0.7}\text{Ca}_{0.3}\text{TiO}_3) - 0.5(\text{BaZr}_{0.2}\text{Ti}_{0.8}\text{O}_3)$
morphotropic composition through multilayer approach**

Soumen Mandi

A Dissertation Submitted to
Indian Institute of Technology Hyderabad
In Partial Fulfillment of the Requirements for
The Degree of Master of Technology



भारतीय प्रौद्योगिकी संस्थान हैदराबाद
Indian Institute of Technology Hyderabad

Department of Materials Science and Metallurgical Engineering

July, 2016

Declaration

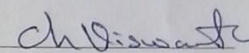
I declare that this written submission represents my ideas in my own words, and where others' ideas or words have been included, I have adequately cited and referenced the original sources. I also declare that I have adhered to all principles of academic honesty and integrity and have not misrepresented or fabricated or falsified any idea/data/fact/source in my submission. I understand that any violation of the above will be a cause for disciplinary action by the Institute and can also evoke penal action from the sources that have thus not been properly cited, or from whom proper permission has not been taken when needed.

Soumen Mandi

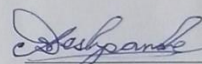
Soumen Mandi
(MS14MTECH11007)

Approval Sheet

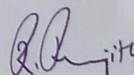
This thesis entitled “Studies on attaining $0.5(\text{Ba}_{0.7}\text{Ca}_{0.3}\text{TiO}_3) - 0.5(\text{BaZr}_{0.2}\text{Ti}_{0.8}\text{O}_3)$ morphotropic composition through multilayer approach” by Soumen Mandi is approved for the degree of Master of Technology from IIT Hyderabad.



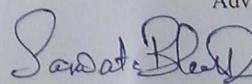
Dr. Vishwanath Chintapenta
Assistant Professor
Department of Mechanical and Aerospace Engineering
Examiner



Dr. Atul Suresh Deshpande
Assistant Professor
Department of Materials Science and Metallurgical Engineering
Examiner



Dr. Ranjith Ramadurai
Assistant Professor
Department of Materials Science and Metallurgical Engineering
Adviser



Dr. Saswata Bhattacharya
Assistant Professor
Department of Materials Science and Metallurgical Engineering
Chairman

Acknowledgements

First and foremost is my sincere gratitude to my guide **Dr. Ranjith Ramadurai** for giving me the opportunity to work under him. From the beginning of the project to the last stage of my stay in IIT Hyderabad his constant encouragement, guidance and advices not only in the area of research field but other prospects of life have now become invaluable to me. No doubt that without his support and motivation I would not have completed the project.

I would like to thank all other faculty members of Department of Materials Science and Metallurgical engineering who shared their knowledge and experiences in and outside the classrooms. They really enhanced my understanding of the subjects.

I also want to thanks all the Ph.d scholars of the department specially **Mr.SajMohan, Mr.Kumarswamy Miriyala, Mr.Bandi Mallesham, Mr.M Venkateshwararao** and my senior **Mr.Mudit Upadhayy** for helping me to learn and perform lab experiments and giving their full attention to all my tiny to huge problems.

Finally a big thanks to all my M.Tech friends who made my life memorable at IIT Hyderabad.

Abstract

The discovery of Piezoelectricity in Quartz in late 1880 by Curie brothers and its technological importance in various fields led to an intense research in this field up to the First World War. Post First World War another class of piezoelectric with perovskite structures was discovered and popularly known was BaTiO_3 . Later the most commercially used materials that ruled the field of piezoelectric based devices and applications was $\text{PbZr}_{0.52}\text{Ti}_{0.48}\text{O}_3$ (PZT). It was commercially successful due to its superior piezo-coefficient and its high Curie temperature. Its importance and vast presence in today's modern world can be estimated by this fact that all major ferroelectric and piezoelectric devices are made up of PZT based compounds. But the growing awareness about human health and environment led world familiar to the hazard that is present by using Lead. So, the need for an alternative lead free piezoelectrics arose. In 2009 Liu and Ren reported a Lead free piezoelectric material with morphotropic composition that have piezo-coefficient value higher than PZT. The compound is known as $\text{Ba}_{0.85}\text{Ca}_{0.15}\text{Zr}_{0.10}\text{Ti}_{0.9}\text{O}_3$ (BCZT) solid solution.

The main objective of our project is to mimic this morphotropic phase composition of $\text{Ba}_{0.85}\text{Ca}_{0.15}\text{Zr}_{0.10}\text{Ti}_{0.9}\text{O}_3$ (BCZT) solid solution through multilayer approach of two $.5(\text{Ba}_{0.7}\text{Ca}_{0.3}\text{TiO}_3) - .5(\text{BaZr}_{0.2}\text{Ti}_{0.8}\text{O}_3)$ individual layers. As the composition is very much complex, pulse laser ablation was a suitable technique to deposit the films. Initially three distinct bulk targets BCT, BZT and BCZT were made of required stoichiometry by solid state synthesis route. Phase formation was confirmed by coupled Θ -2 Θ X Ray Diffraction. These targets were then used to deposit polycrystalline films on platinum (111) coated silicon substrate in optimized conditions. Thin films phase were characterized by GIXRD. Then atomic force microscopy (AFM) and piezo-response force microscopy (PFM) study was done to know the surface morphology and ferroelectric behaviour of the films. To know the dc leakage behaviour of the thin films I-V measurements was performed at room temperature. Our study shows that the BCZT thin film deposited at 650°C possess strong ferroelectric nature and least leakage current in compare to all other films.

Nomenclature

BT-Barium titanate

KDP-Potassium dihydrogen phosphate

PZT-Lead zirconate titanate

BCT-Barium calcium titanate

BZT-Barium zirconate titanate

BCZT-Barium calcium zirconium titanate

MPB-Morphotropic phase boundary

T_c -Curie temperature

XRD-X ray diffraction

GIXRD-Grazing incidence x ray diffraction

PLD-Pulse laser deposition

AFM-Atomic force microscopy

PFM-Piezo-response force microscopy

JCPDS-Joint committee on powder diffraction standards

PVA-Polyvinyl alcohol

Content

Declaration.....	ii
Approval sheet.....	iii
Acknowledgements.....	iv
Abstract.....	v
Nomenclature.....	vi
1 Introduction.....	1-7
1.1. Ferroelectricity.....	1
1.2. Origin of ferroelectricity.....	2-3
1.3. Piezoelectricity	3
1.4. Piezoelectric coefficients.....	4
1.5. Piezoelectricity brief history.....	5
1.6. Piezoelectric materials.....	5
1.5.1 Lead based piezoelectric materials.....	6
1.5.2 Lead free piezoelectric materials.....	7
1.5.3 Objective.....	7
2 Literature review	8-11
2.1 Barium Titanate.....	8
2.2 Effect of Zirconium on Barium Titanate.....	9
2.3 Effect of Calcium on Barium Titanate.....	9-10
2.4 Barium Calcium Zirconium Titanate.....	11
3 Experimental details.....	12-17
3.1 Preparation of BCT bulk target.....	12-13
3.2 Preparation of BCT bulk target.....	13-14
3.3 Preparation of BCZT bulk target.....	15-16
3.4 Fabrication of BCZT, BZT, BCT and BCT/BZT bilayer thin films in PLD.....	16-17
4 Characterization techniques.....	18-23

4.1 X-Ray Diffraction.....	18
4.2 Grazing Incidence XRD.....	19
4.3 Atomic Force Microscopy.....	20-21
4.4 Piezo-force Microscopy	21-22
4.5 V-I characterisation.....	22-23
5 Results and Discussion.....	24-39
5.1 Structural Characterisation of BCT, BZT, BCZT bulk targets and the polycrystalline thin films.....	24-30
5.2 Surface morphological studies with Atomic force microscopy.....	30-32
5.3 Ferroelectric behaviour Studies with Piezoforce microscopy.....	32-35
5.4 Leakage current comparison.....	36-39
6 Summary and conclusions.....	40
6.1 Summary.....	40
6.2 Conclusions.....	40
6.3 Future work.....	41
References.....	42

Chapter 1

INTRODUCTION

1.1 FERROELECTRICITY

Materials which exhibit ferroelectricity possess spontaneous polarization and can switch their polarization direction on applying an external electric field. They have a polarization hysteresis loop analogous to ferromagnetic materials with magnetic hysteresis. Non-centro symmetry in the crystal system is one of the essential criteria for a material to possess ferroelectric property [1]. The ferroelectric property of any material is temperature and crystal structure dependent.

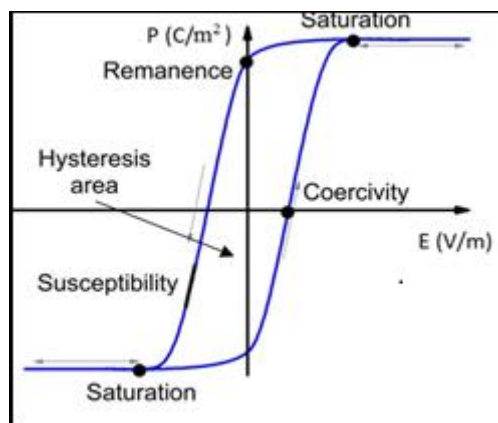


Fig 1.1 Hysteresis Loop[2]

1.2 Origin of ferroelectricity

The origin of ferroelectricity is due to three major factors: (1) Hydrogen bond (KH_2PO_4) (2) rattling of cation (BaTiO_3) and (3) Lone pair effect (BiFeO_3 , PbTiO_3).

(1) Hydrogen bond

KH_2PO_4 (KDP) is a prototype crystal belonging to the family of hydrogen bonded ferroelectric materials. The PO_4 tetrahedra units are interconnected by planar hydrogen bonds and ferroelectricity originates due to the position of proton in these Hydrogen bonds. Above Curie temperature, the H-atoms occupy with equal probability two symmetrical positions along the H-bond separated a distance δ , which characterizes the disordered phase. Below the critical temperature $T_c \approx 122$ K, the protons localize into one of the symmetric sites, thus leading to the ordered Ferroelectric phase. The proton configuration in this phase is shown below in Fig1.2; each PO_4 unit has two covalently bonded and two H-bonded hydrogen atoms [3].

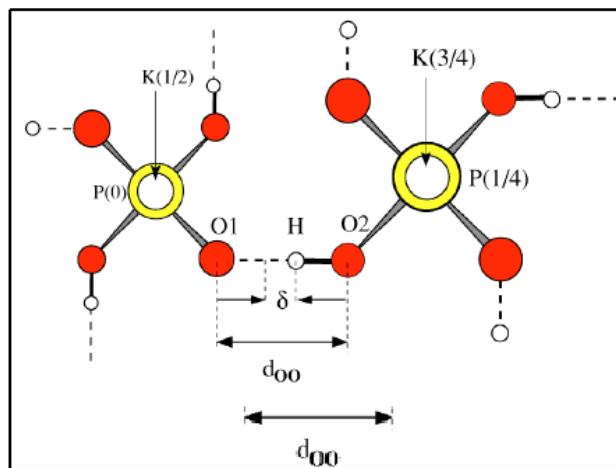


Fig 1.2 Schematic view of KDP internal structure. Covalent bond and hydrogen bond are represented in solid and dashed lines [3]

(2) Rattling of B-cation in ABO_3 structures

Rattling of B-Cations could be found in perovskite structure having a formula unit of ABO_3 type. The first ferroelectric perovskite material to be discovered was BaTiO_3 (BT). The core of the cubic ABO_3 lattice is formed by an oxygen octahedron with a B^{4+} cation at the centre. The A^{2+} ions are at the corners of the unit cell which gives the neutrality and structural stability. The ferroelectric and piezoelectric property is acquired by this material below Curie temperature i.e. due to rattling of B^{4+} ion in the BO_6 octahedron. Above Curie temperature the material behaves as a para-electric [4].

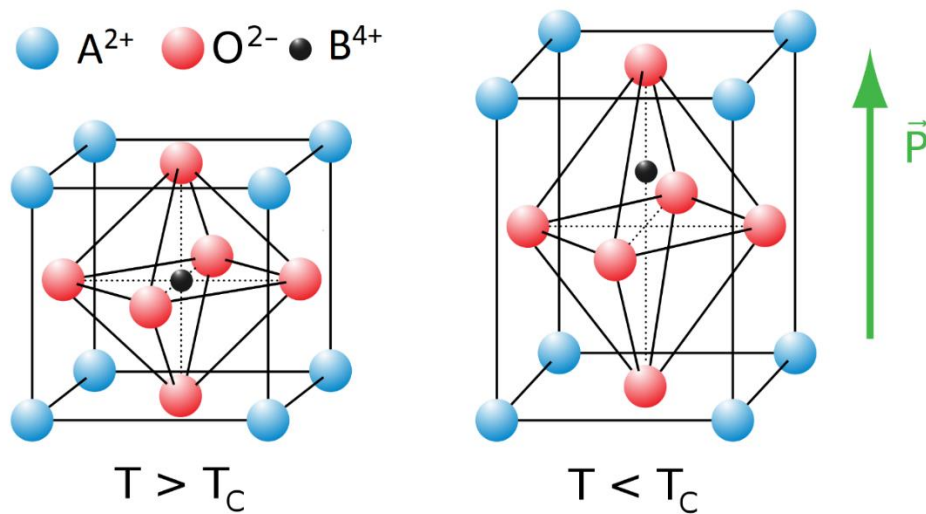


Fig 1.3 (a) Perovskite structure (b) Rattling of cation in BO_6 octahedra [5]

(3) Lone pair effect

This effect is found when the A cation of the perovskite crystal is substituted by either Lead (Pb^{2+}) or Bi^{3+} ion with respective B-cations. In the $BaTiO_3$ phase the interaction between the oxygen and barium atom is completely ionic whereas in $PbTiO_3$ there is a strong hybridization between lead 6s and oxygen 2p states.[6] The electron lone pair is not symmetrically distributed around the Pb ion but is localized along the $\langle 111 \rangle$ direction in the $PbTiO_3$ unit cell. This leads to the off centering of the titanium ion from the center of the unit cell due to charge repulsion. This gives rise to the strong ferroelectric property in this system [6].

1.3 PIEZOELECTRICITY

The ferroelectric materials also have a interesting property known as *Piezoelectricity*.

Piezoelectricity is the ability of a material to get polarized under applied mechanical pressure and vice-versa.

1.4 Piezoelectric coefficients

DIRECT PIEZO-EFFECT : When a mechanical stress is applied to generate electric polarisation is known as direct piezo-effect.

$$\mathbf{P}_i = \sum \mathbf{g}_{ij} \sigma_j \quad \dots (1)$$

Here, \mathbf{g}_{ij} is a second rank tensor known as *piezoelectric strain constant* expressed in nC/N. Because a piezoelectric ceramic is anisotropic, physical constants relate both to direction of mechanical or electric force. The subscripts \mathbf{i} & \mathbf{j} represent the direction of polarisation and strain respectively. Directions X, Y, Z is represented by the subscript 1, 2, 3 and shear about this axes are represented by the subscript 4, 5, 6.

CONVERSE PIEZO-EFFECT: When an applied electrical field induces a strain in the material is known as converse piezo-effect.

$$\boldsymbol{\varepsilon}_i = \sum \mathbf{d}_{ij} \mathbf{E}_j \quad \dots (2)$$

The tensor \mathbf{d}_{ij} is known as *piezoelectric voltage constant* whose unit is pm/V.

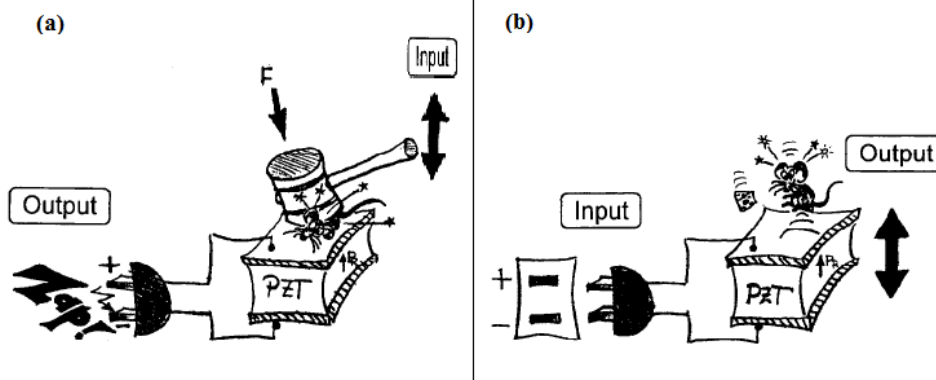


Fig 1.4 (a) Direct effect (b) Converse effect [7]

ELECTROMECHANICAL COUPLING FACTOR: It is the efficiency of the ceramic material to convert electrical energy into mechanical energy or vice-versa.

$$k^2 = \frac{\text{mechanical energy stored}}{\text{electrical energy applied}} \dots\dots(3)$$

Quartz was the first mineral in which Curie brothers (Pierre and Jacques curie) discovered the direct piezoelectric effect in 1880 but they did not predict the converse piezoelectric effect. In the following year 1881 Mr. Gabriel Lippman mathematically deduced from fundamental thermodynamic principles the converse piezoelectric effect [7]. The Curie's later confirmed the existence of this effect.

The first serious applications work on piezoelectric devices took place on World War 1. In 1917, P.Langevin and French co-workers began to design an ultrasonic submarine detector to detect or locate a distant submarine in the sea against German menace. It consist of thin single crystal quartz sandwiched between two steel plates. Contemporarily another piezoelectric material Rochelle salt (RS) ($\text{NaKC}_4\text{H}_4\text{O}_6 \cdot 4\text{H}_2\text{O}$) which was technically more efficient than Quartz at that span of time. But RS crystals are unstable and deteriorate easily either by dehydration or by dissolving in water. During the World War 2, the discovery of BaTiO_3 as a high dielectric material replacing mica & TiO_2 used in capacitors and subsequently its superior piezoelectric properties over Quartz and Rochelle Salt triggered an intense research and development in barium titanate ceramic family which led to the lead-titanium-zirconium alloy (PZT) [7] .Today the most important piezoelectric materials that are technologically important are ferroelectric ceramics based on Pb-containing perovskites. But the growing concern over Lead toxicity towards environment and human health is driving to find an effective alternative material other than PZT.

1.5 PIEZOELECTRIC MATERIALS

Piezoelectric materials that are commercially more used are made up of quartz and lead based perovskite ceramics. But there are many other piezoelectric materials available such as barium titanate, lithium niobate, gallium orthophosphate, piezo-polymers (PVDF, polystyrene, polypropylene). Among all these known piezoelectric materials lead based perovskites ceramics exhibits superior properties and dominates the application.

1.5.1 Lead based piezoelectric materials

Lead zirconium titanate (PZT)

Lead zirconium titanate is a solid solution of PbTiO_3 and PbZrO_3 . The solid solution $\text{Pb}(\text{Zr}_x\text{Ti}_{1-x})\text{O}_3$ has the perovskite crystal structure with Zr^{4+} ion substituted randomly at the Ti^{4+} ion positions. This solution exhibits a very interesting ferroelectric and piezoelectric property when equal amount of PbTiO_3 and PbZrO_3 are present in the binary solid solution. The phase boundary that separates PZT crystal structure at almost equal amounts of PT and PZ is known as morphotropic phase boundary. In the vicinity of the MPB a composition dependent phase transition occurs in which the Ti-rich tetragonal phase changes to Zr-rich rhombohedral phase having $T_c > 300^\circ\text{C}$ which implies high operating temperatures for PZT ceramics. The Piezo coefficient d_{33} value is 600pC/N near the MPB [8]. It is due to same free energy of the tetragonal and rhombohedral phase in the vicinity of MPB which decreases the energy barrier for switching the polarisation direction vector and the number of polarisation directions also increases due to existence of both the phases [9].

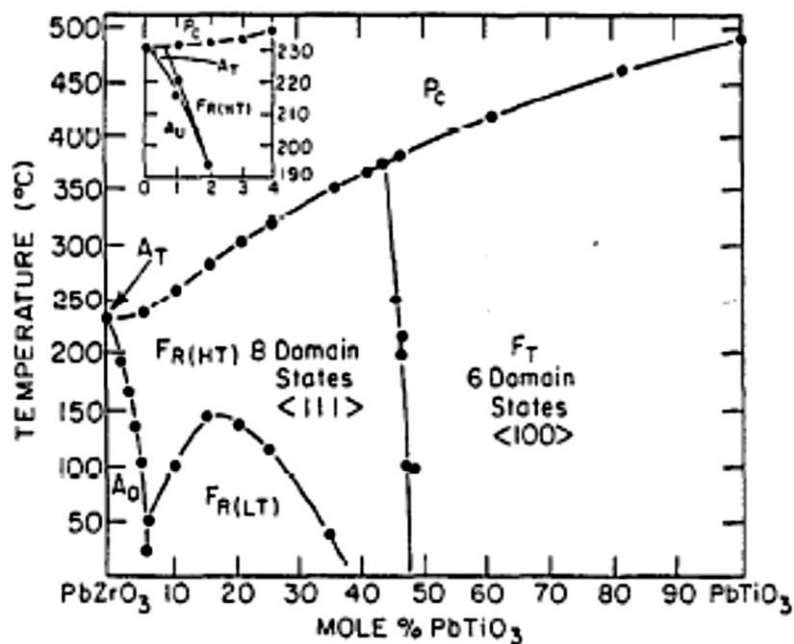


Fig 1.5 Phase diagram of PbZrO_3 - PbTiO_3 [8]

1.5.2 Lead free piezoelectric materials

The most extensively studied lead free piezoelectric is barium titanate. But barium titanate piezo coefficients are very much less in compare to Lead based perovskites and its Curie temperature is only 120°C which limited its further application at high temperatures. To enhance its properties numerous

studies have been done by substituting several elements at A-site and B-site position. Among them the most promising material is barium calcium zirconium titanate (BCZT). In this material the Ca²⁺-ion occupies the Ba²⁺ site and Zr⁴⁺-ion occupies the Ti⁴⁺-site. Also the binary solid solution of BCT-BZT possess a morphotropic phase boundary similar to lead based binary solid solution. In BCZT composition near MPB researchers have found d_{33} value up to 620 pC/N but the Curie temperature is around 93 ° C only [10]. In this project we have aimed at fabrication of thin films of BCZT morphotropic composition and study the piezoelectric properties.

OBJECTIVE OF THE PROJECT

- Preparation of BCT, BZT and BCZT bulk target by solid state synthesis
- Optimization and fabrication of BCT, BZT and BCZT thin film by Pulse Laser Deposition
- Multilayer approach to mimic Morphotropic Phase Boundary Features (Piezoresponse dielectric phase transition, Leakage current measurment)
- Phase formation confirmation with the help of XRD
- Morphological and Domain analysis with Atomic force microscopy and Piezoresponse force microscopy

Chapter 2

LITERATURE REVIEW

2.1 Barium Titanate (BaTiO_3)

Barium Titanate (BT) is the first ferroelectric perovskite ceramic to be discovered. The core of the essential cubic BT lattice cell is formed by an oxygen octahedron with a 4-valent titanium ion at the centre. The 2-valent barium ions are at the corner of the unit cell which gives the neutrality and structural stability as shown in fig2.1. The ferroelectric and piezoelectric property is acquired by this material below Curie temperature i.e. 120°C is due to rattling of Ti^{4+} ion in the TiO_6 octahedron. Above 120°C BT is cubic and below, it transform successively to three ferroelectric phases: first to $4mm$ tetragonal, then to mm orthorhombic at about 5°C and finally to a $3m$ rhombohedral phase below -90°C . The polar axis in the three ferroelectric phases are in $\langle 001 \rangle$, $\langle 110 \rangle$, and $\langle 111 \rangle$ directions for tetragonal, orthorhombic and rhombohedral structures respectively as shown in fig2.2. [11]

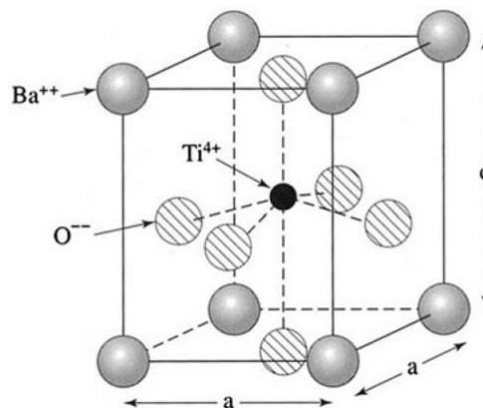


Fig 2.1 BaTiO_3 crystal structure[12]

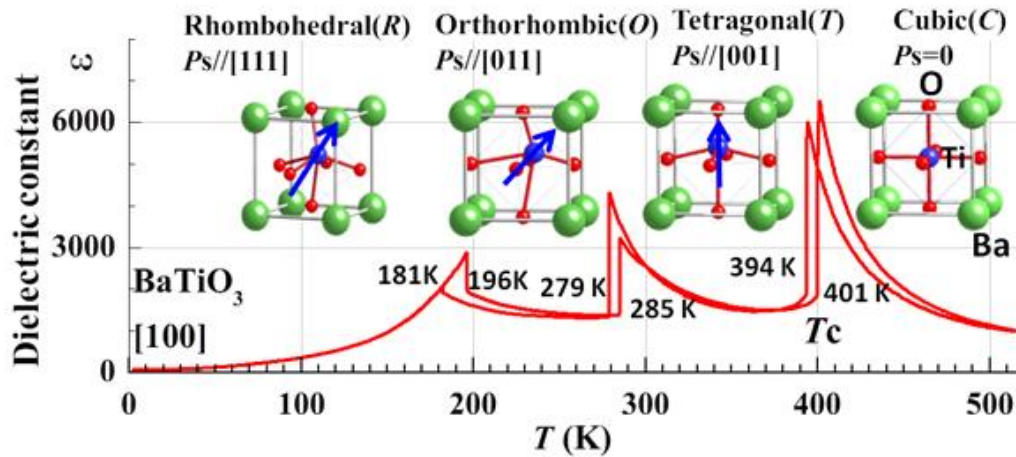


Fig 2.2 Phase transition of BaTiO₃ vs Temperature[13]

2.2 Effect of Zr on BaTiO₃

The titanium tetra-valent ion can be substituted by Zirconium tetra-valent ion in the solid solution of barium titanate. The ionic radius of Zr⁴⁺ ion is 72pm [14] which is larger than the ionic radius of Ti⁴⁺ ion (60.5pm)[14] due to which there is an expansion of the perovskite lattice. It is also chemically more stable than titanium and there is a strong hybridisation between Zirconium and Oxygen atoms which increases the band gap of the material as a result it reduces the leakage current. The addition of Zirconium decreases the average grain size.

With the addition of Zirconium the Curie temperature of the Barium titanate decreases. But there is an enhancement in dielectric values, increases both the saturation polarization and remnant polarization. The ferroelectric properties in the BaZr_xTi_{1-x}O₃ system have been investigated for several concentration of Zr and the study shows that for the composition $0 \leq x \leq 0.1$ ceramics shows normal ferroelectric behaviour. However for compositions $0.25 \leq x \leq 0.75$ ceramics shows a relaxor behaviour. The relaxor region $0.25 \leq x \leq 0.75$ can be further divided into two types: Type I and type II. Type I is Ti rich phase dominated by the polar BaTiO₃ clusters and the T_m decreases with increase in Zr concentration. Type II region is Zr rich phase dominated by non-polar BaZrO₃ and the T_m remains almost constant with increase in Zr value [15]. The phase diagram of BaZr_xTi_{1-x}O₃ based on the dielectric permittivity is shown below:

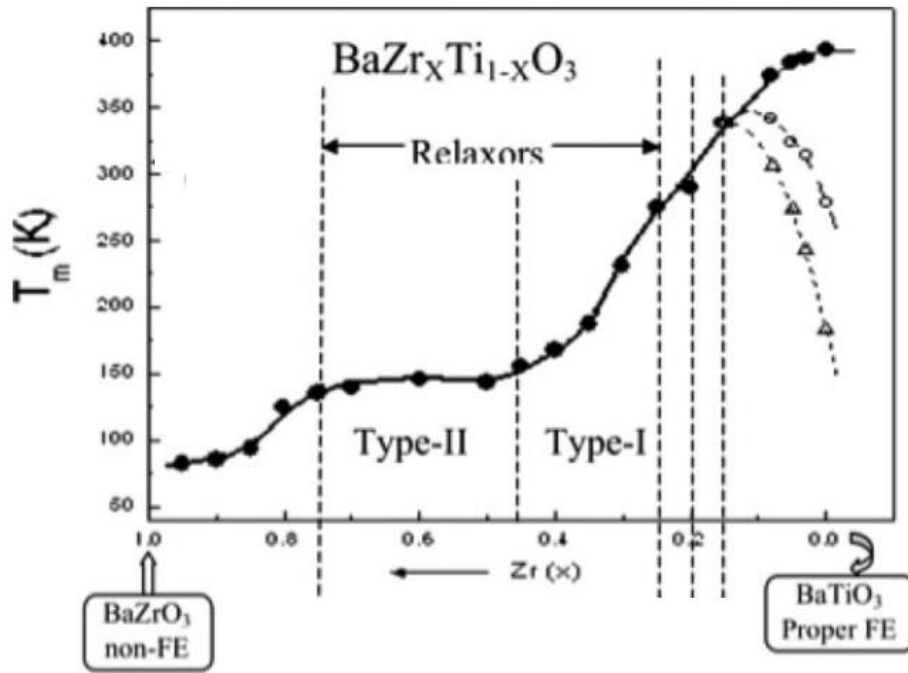


Fig 2.3 Phase diagram of $\text{BaZr}_x\text{Ti}_{1-x}\text{O}_3$ [15]

2.3 Effect of Ca in BaTiO_3

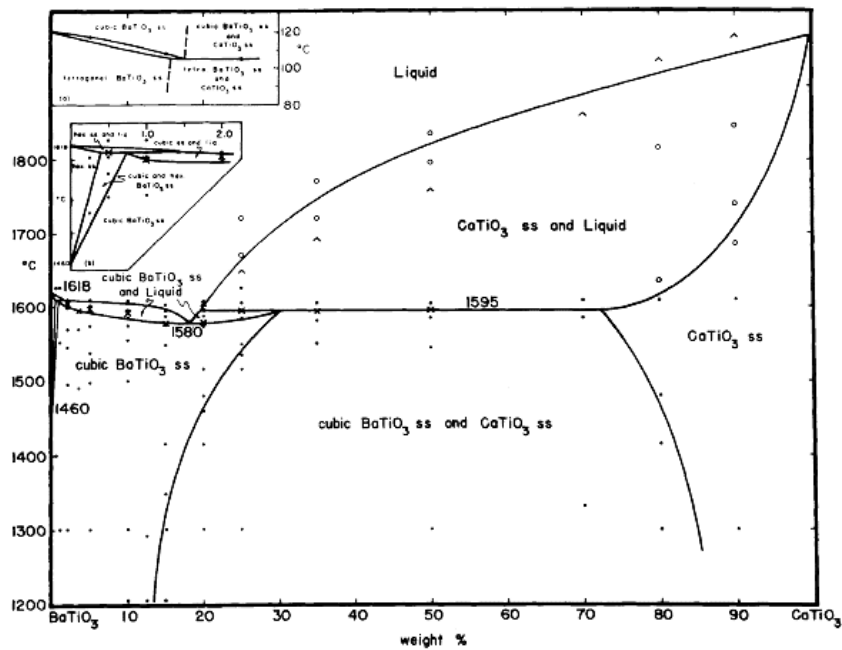


Fig 2.4 Phase diagram of BaTiO_3 - CaTiO_3 . Left side top shows the lowering of Curie temperature with increase of Ca conc[16]

The Ca^{2+} ion is substituted at Ba^{2+} ion in the solid solution of BaTiO_3 . The maximum solubility limit of Calcium in Barium titanate is 30% at 1600°C as shown below in the phase diagram [16]. The Curie temperature decreases with increase in Calcium concentration in the BaTiO_3 . By the incorporation of Ca ions at Ba ion position the unit cell volume decreases as ionic size of Ca^{2+} (134pm)[14] is lower than the Ba^{2+} ions (161pm)[14]. To maintain the structural stability there is an octahedral tilt in the BO_6 cage which will tend to increase the Ti off centering and an increase in saturation polarization is observed.

2.4 Barium calcium zirconium titanate (BCZT)

In order to match the high piezoelectric coefficient that is found in Lead based ferroelectric materials, Wenfeng Liu and Xiaobing Ren in 2009 successfully reported a non-Pb piezoelectric system BZT-BCT which possess a Morphotropic Phase boundary similar to lead based compounds having a piezoelectric coefficient of 620pC/N at MPB which is even higher than Pb based materials. But the Curie temperature is 93°C which is very much less than lead based materials. There is a tri-critical point in the BZT-BCT system at $x=0.35$ and $T=57^\circ\text{C}$ where the polarisation anisotropy vanishes due to similar free energy [10]. The phase diagram for BZT-BCT is shown below:

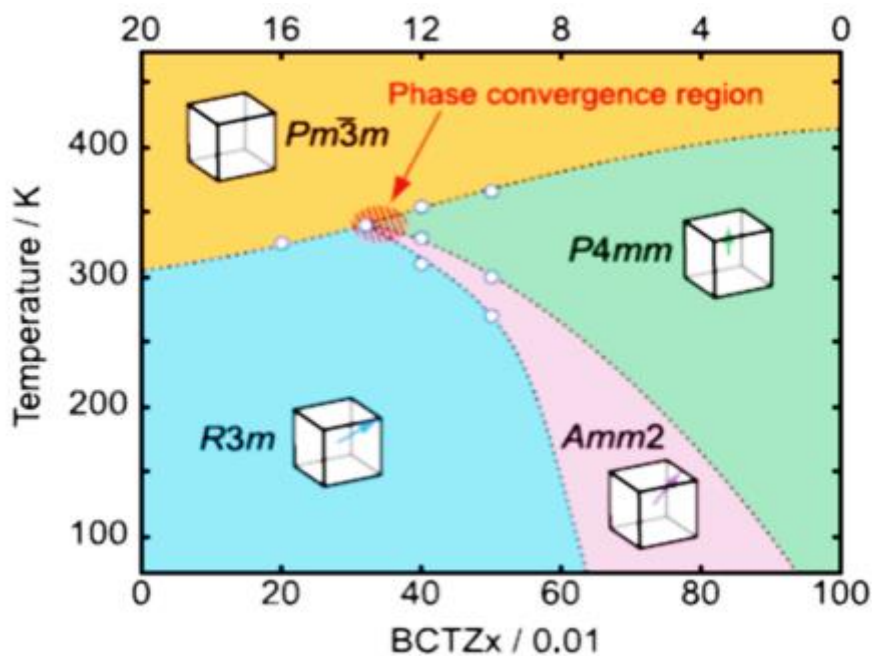


Fig 2.5 Phase diagram of BCZT [17]

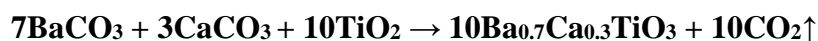
Chapter 3

EXPERIMENTAL

Pulse Laser Ablation is the deposition technique that had been used to deposit thin films. Prior to depositing thin films separate bulk target materials had been prepared for BCT, BZT and BCZT (0.5BCT – 0.5BZT) through solid state synthesis route. The films for the respective targets were deposited under optimum conditions. Later on XRD, AFM, PFM, V-I measurement and dielectric characterization were done on the films.

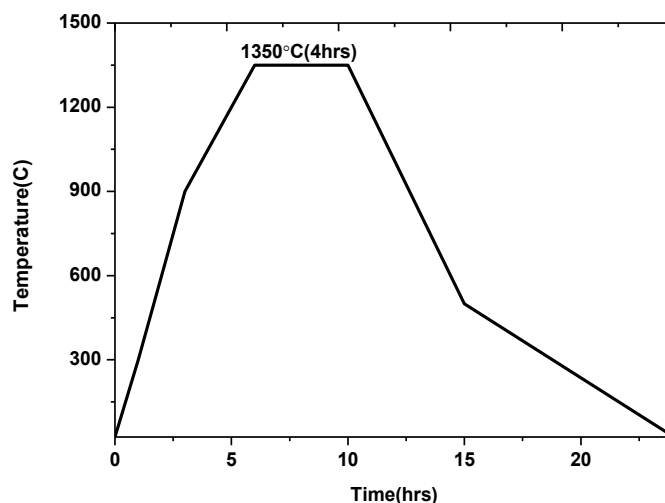
3.1 Preparation of BCT target

The starting raw materials to prepare BCT target were BaCO₃, CaCO₃ and TiO₂. The chemical reaction that occurs is given below:

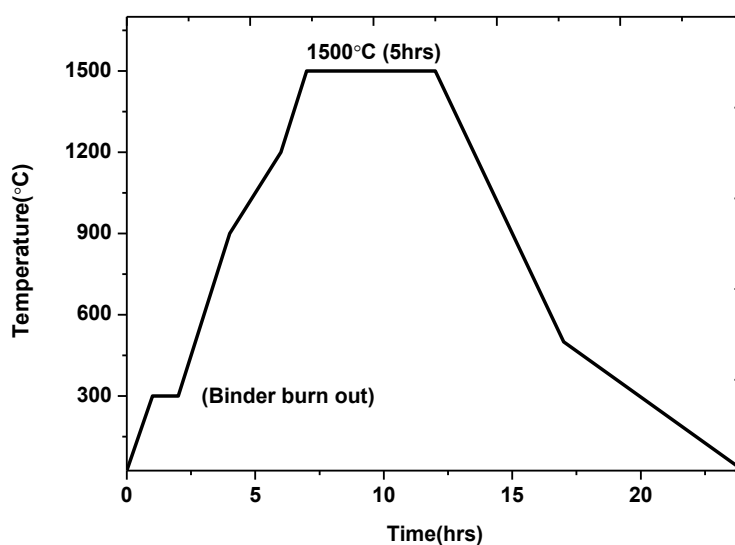


Steps involved:

1. All the chemical powders were taken in their stoichiometric ratios. They were mixed and hand ground for 5hours in agate motor.
2. Calcination-The mixed powder was poured in an alumina crucible and kept inside a muffle furnace for phase formation at 1350°C for 4hours. The calcination profile is shown below:

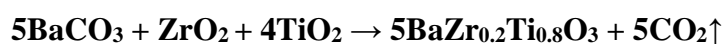


3. The phase formation of the calcined powder was studied by X Ray Diffraction technique.
4. The calcined powder was again hand ground for 10hrs in agate motor. Later it was mixed with PVA(Polyvinyl alcohol) binder and pressed into a pellet of 20mm diameter at a pressure of 4Tons for 1min using a hydraulic press.
5. Sintering- The pellet was sintered at 1500°C in muffle furnace for 5hours for densification. It was hold at 300°C for 1hour for complete removal of binder. The sintering profile is shown below:



3.2 Preparation of BZT target

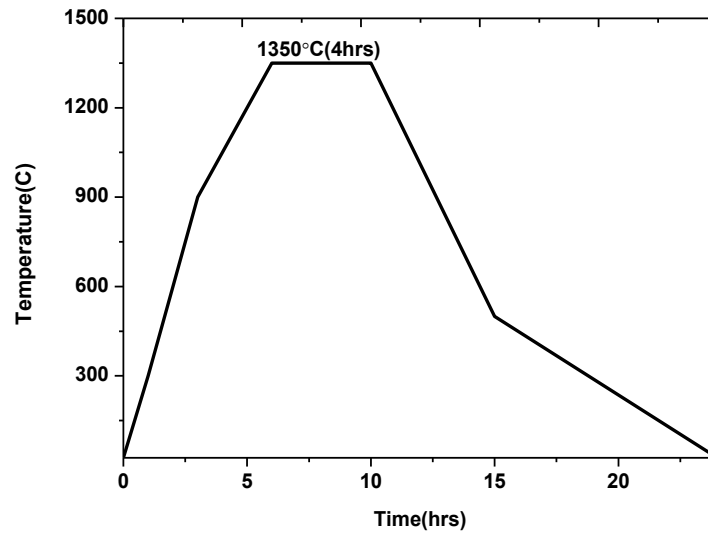
The starting materials to prepare BZT target were BaCO₃, ZrO₂ and TiO₂. The chemical reaction that occurs is



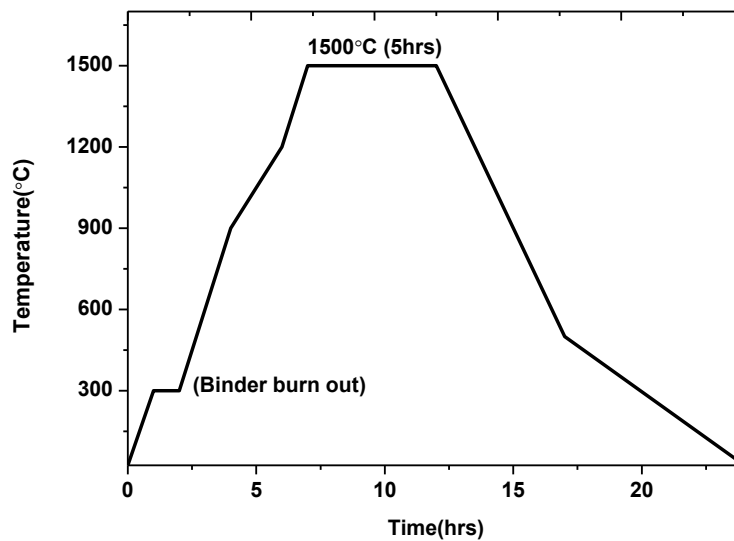
Steps involved:

1. All the chemical powders were taken in their stoichiometric ratios. They were mixed and hand ground for 5hours in agate motor.

2. Calcination-The mixed powder was poured in an alumina crucible and kept inside a muffle furnace for phase formation at 1350°C for 4hours. The calcination profile is shown below:

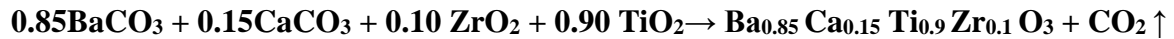


3. The phase formation of the calcined powder was studied by X Ray Diffraction technique.
4. The calcined powder was again hand ground for 10hrs in agate motor. After that it was mixed with PVA(Polyvinyl alcohol) binder and hydraulically pressed into a pellet of 20mm diameter at a pressure of 4Tons for 1min.
5. Sintering- The pellet was sintered at 1500°C in muffle furnace for 5hours for densification. It was hold at 300°C for 1hour for complete removal of binder. The sintering profile is shown below:



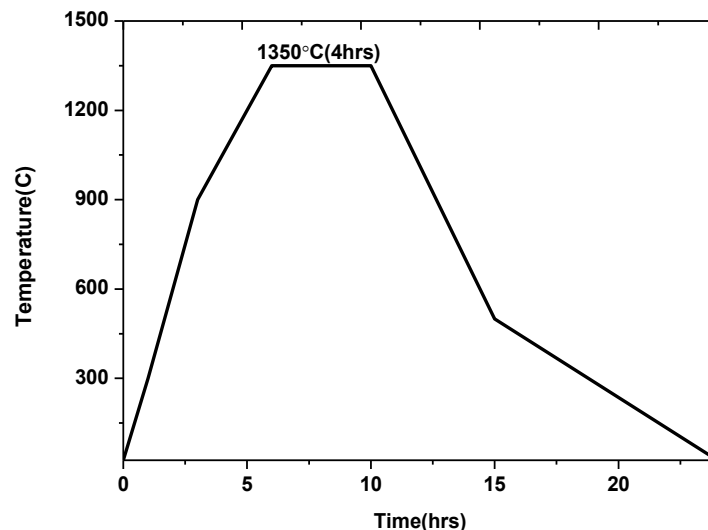
3.3 Preparation of BCZT target

The starting materials to prepare BZT target were BaCO₃, ZrO₂, CaCO₃ and TiO₂. The chemical reaction that occurs is

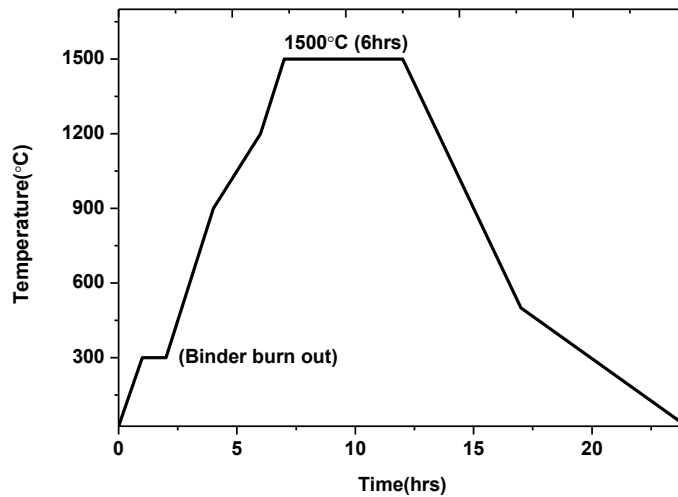


Steps involved:

1. All the chemical powders were taken in their stoichiometric ratios. They were mixed and hand ground for 5 hours in agate motor.
2. Calcination-The mixed powder was poured in an Alumina crucible and kept inside a muffle furnace for phase formation at 1350°C for 4 hours. The calcination profile is shown below:



3. The phase formation of the calcined powder was studied by X Ray Diffraction technique.
4. The calcined powder was again hand ground for 10hrs in agate motor. After that it was mixed with PVA (Polyvinyl alcohol) binder and hydraulically pressed into a pellet of 20mm diameter at a pressure of 4Tons for 1min.
5. Sintering- The pellet was sintered at 1500°C in muffle furnace for 6hours for densification. It was hold at 300°C for 1hour for complete removal of binder. The sintering profile is shown below



NOTE: Separate crucibles were used for preparation of each targets.

3.4 Deposition of BCZT/BZT/BCT thin films on Pt(111)/TiO₂/SiO₂/Si substrate

BCZT, BZT and BCT thin films were deposited on platinum coated silicon substrate using Pulse Laser Deposition technique.

Pulse Laser Deposition

Pulse Laser Deposition is a versatile technique which is vastly used to deposit materials of complex stoichiometry especially multi-component oxides. The schematic view of a PLD system is shown below in fig3.1:

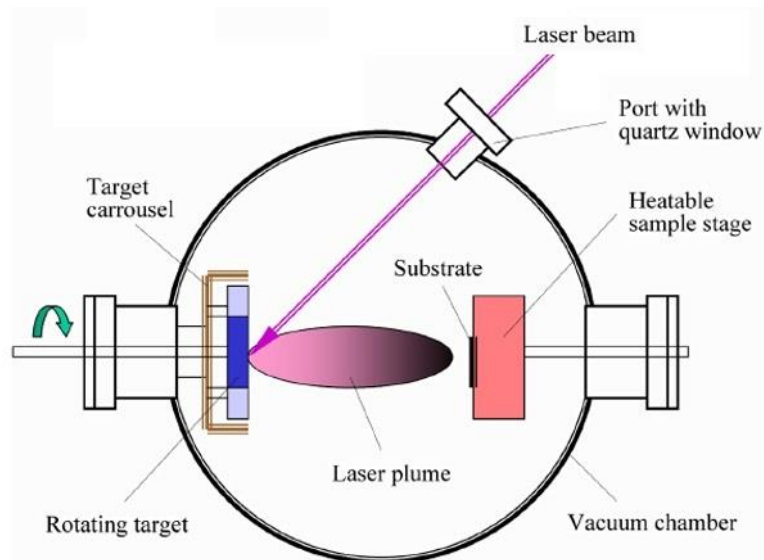


Fig 3.1 PLD Set up[18]

In this schematic diagram the rotary pump and the turbo pump(high vacuum pump) is not shown which is a pre-requisite to create vacuum in the chamber before deposition.

Process

A high power pulsed laser is focused onto the rotating target material (can be of multi-target system) inclined at 45 degree with respect to target normal and when the laser fluence exceeds the ablation threshold for the material, the material locally melts. Chemical bonds are broken and the backward thrust experienced by the melt results in a forward ejection of the species called as plume which is a mixture of neutral atoms, molecules, ions and solid debris. The plume expands towards a substrate surface in vacuum under a reactive atmosphere which is not always essential before getting deposited. The sample stage holder is usually provided with a heating arrangement for optimizing thin film nucleation and growth conditions[18]. The other control parameters that affect the quality of the films are as follows:

- a) Density and composition of the target material
- b) Laser energy density
- c) Pulse frequency
- d) Pressure in vacuum chamber and the type of gas
- e) Target to substrate distance
- f) Substrate temperature
- g) Cooling rate
- h) Substrate choice

Chapter 4

Characterization techniques

The characterisation techniques that had been used for the analysis of the samples involves X-Ray Diffraction (XRD), Grazing Incidence XRD (GIXRD), Atomic Force Microscopy (AFM), Piezo-force Microscopy (PFM), V-I characterisation.

4.1 X-RAY DIFFRACTION

X-ray diffraction is commonly used to study crystal structures and atomic spacing. The use of X-rays is very specific because the inter-planar distance in crystals act as a diffraction grating for X-ray wavelength. This technique is basically based on the principle of **Bragg's law** which is

$$2d\sin\theta = n\lambda$$

Where d = inter-planar spacing in crystal

θ = angle of diffraction

λ = wavelength of X-ray (common X-ray target source is **CuK_α**=1.5418Å)

The Figure 4.1 geometrically represents the X-ray reflection phenomenon in crystals:

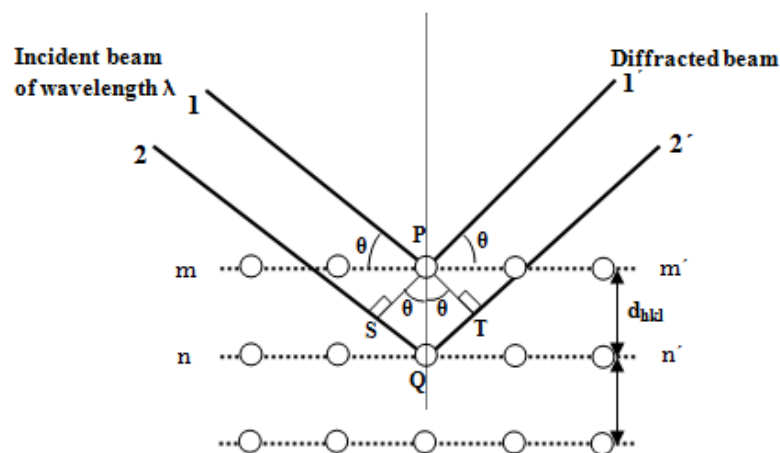


Fig 4.1 Schematic detailing the Bragg's reflection condition [19]

This law states that the Bragg reflected ray undergoes a constructive interference whenever the Bragg's condition is satisfied[20]. By scanning the sample for required 2θ angles, all possible diffraction directions can be achieved due to random orientation of the crystals. And we know that each element has its own specific d-spacings ,so by comparing with standard reference patterns i.e JCPDS files we can determine the phases.

4.2 GRAZING INCIDENCE XRD

Conventional θ - 2θ scanning is not suitable for analysing thin films as it generates a very weak signal from the film and an intense signal from the substrate.

The schematic for GIXRD is shown below:

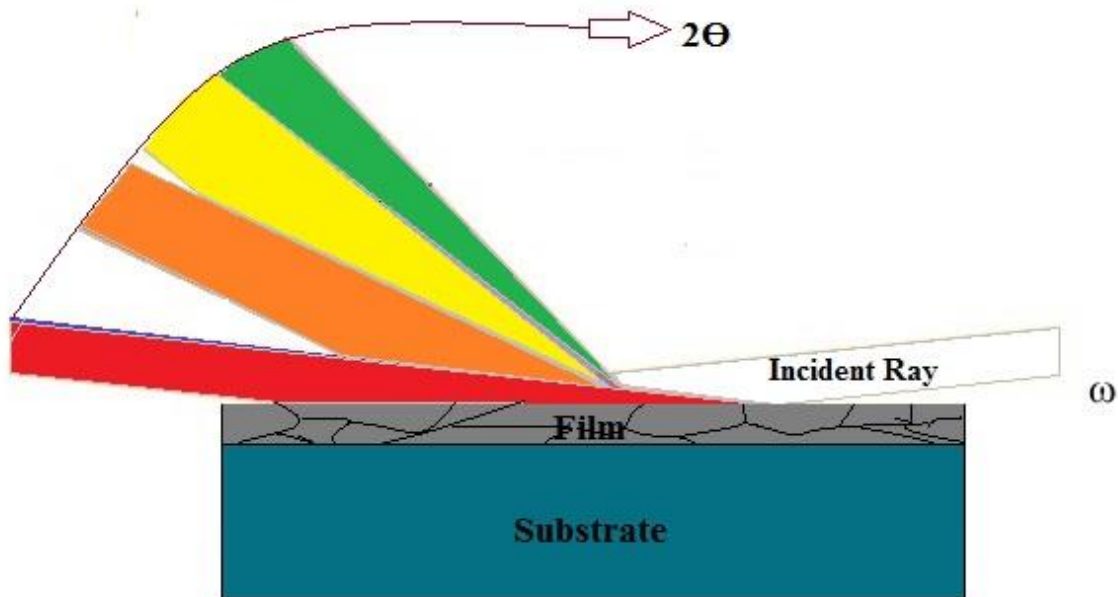


Fig. 4.2 Schematic explaining the grazing incidence of X-ray and diffraction pattern[21].

In the GIXRD, incident rays is fixed at small grazing angle ω and 2θ scanning is done. As a result the diffraction pattern becomes very much surface sensitive and intensifies the film signal. The signals coming from the substrate can be minimised by varying the grazing angle[21].

4.3 ATOMIC FORCE MICROSCOPY

Atomic force microscopy works basically on the basis of Lennard-Jones potential as shown below:

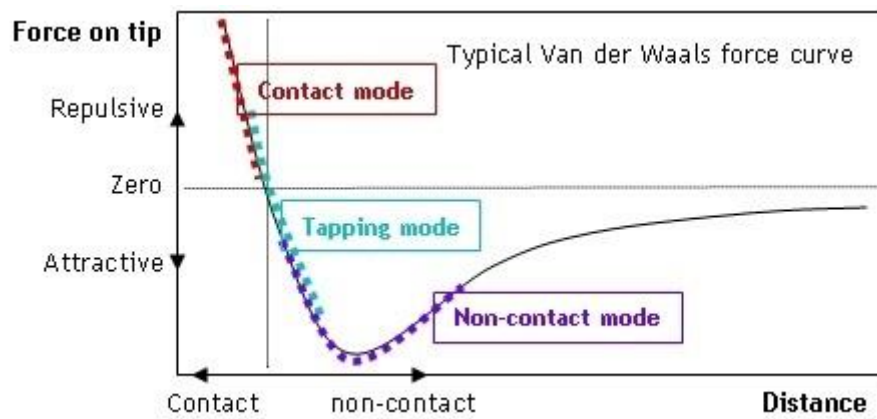


Fig 4.3 Variation of Lennard Jones Potential with respect to interatomic distance[22]

The schematic instrumental set up generally used can be shown as:

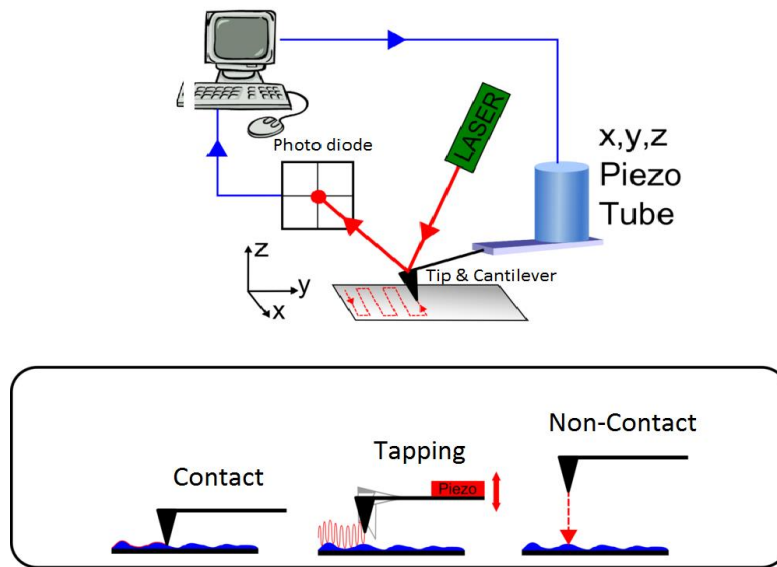


Fig 4.4 Schematic of AFM and its operating modes [23]

The main components of AFM is (a) Tip & Cantilever (b) Piezo scanner (c) Photo diode detector (d) Laser (e) Feedback control & computer.

The common use of AFM is to analyse surface morphology. It acts on the basis of Lennard –Jones potential which can be mathematically formulated as

$$V(r) = 4\epsilon \left[\left(\frac{\sigma}{r} \right)^{12} - \left(\frac{\sigma}{r} \right)^6 \right]$$

The first term $4\epsilon \left(\frac{\sigma}{r} \right)^{12}$ and the second term $-4\epsilon \left(\frac{\sigma}{r} \right)^6$ represents the Repulsive and Attractive potential respectively. Here ϵ is the depth of the potential well, σ is the finite distance where inter particle potential is zero and r is the separation between the two particles.

As the tip scans the surface of the sample, according to the topography of the sample the tip will suffer deflection which is detected by the laser beam deflection in the photodiode which is initially aligned and fixed at a particular set point. The error generated by the deflection in the photodiode will be sent to the feedback loop system which will try to again bring the tip at the fixed set point with the help of Piezo scanner attached with the cantilever and tip. Thus by measuring this deflection, the surface morphology of the sample can be obtained.

4.4 PIEZORESPONSE FORCE MICROSCOPY

Piezoresponse force microscopy (PFM) is used for imaging domain patterns in a ferroelectric material. It works based on the converse piezoelectric effect, which is when a voltage is applied to a piezo material a strain will be generated in the material.

It is a variant of atomic force microscopy which is operated in a contact mode with an applied A.C voltage applied to the conductive tip which exceeds locally the coercive field of the sample. In response to the applied electric field the sample locally expands or contracts according to the polarisation direction or domain direction. The electromechanical deformation is transmitted sensitively by the cantilever bending to the position sensitive photodiode. The error that is produced in the photodiode is then demodulated by the lock in amplifier (LIA) and imaging is done [24, 25] .The schematic diagram for PFM is shown below in fig4.5:

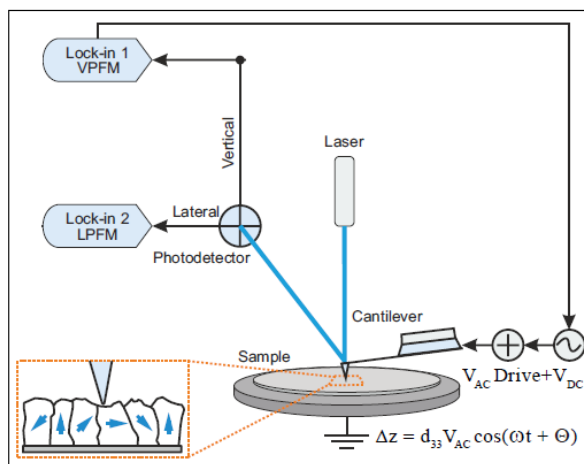


Fig4.5 Schematic for contact mode PFM[24]

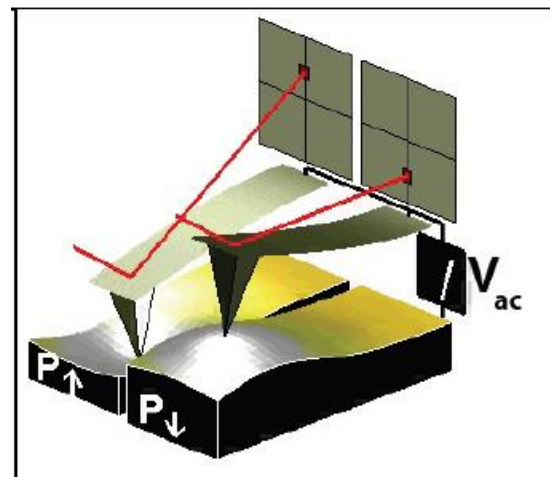


Fig 4.6 Polarisation dependence on sample strain on + bias at tip [25]

4.5 V-I Characterisation

To study the Current-Voltage behaviour (V-I) or the leakage current all the films were fabricated in metal –insulator-metal configuration. The delay time is 0.5sec and holding time is null. The top and

bottom electrode are Platinum. Circular dots of 500 μ m size were deposited on top of films by E-beam evaporation technique as shown below in figure4.7:

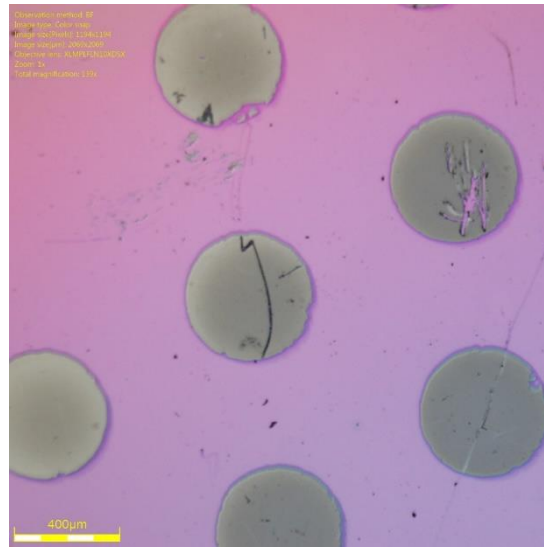


Fig4.7 Platinum circular dots of 500 μ m size deposited by E beam evaporation technique

Chapter 5

RESULTS AND DISCUSSIONS

5.1 Structural characterisation of BCZT, BZT and BCT bulk and their polycrystalline thin films with XRD

BCZT, BCT and BZT powders were calcined at 1350°C and densified in the form of pellets by sintering at 1500°C in air. The bulk structural characterisation was done by XRD operating in a coupled Θ - 2Θ mode in Bragg-Brentano geometry.

BCZT Target

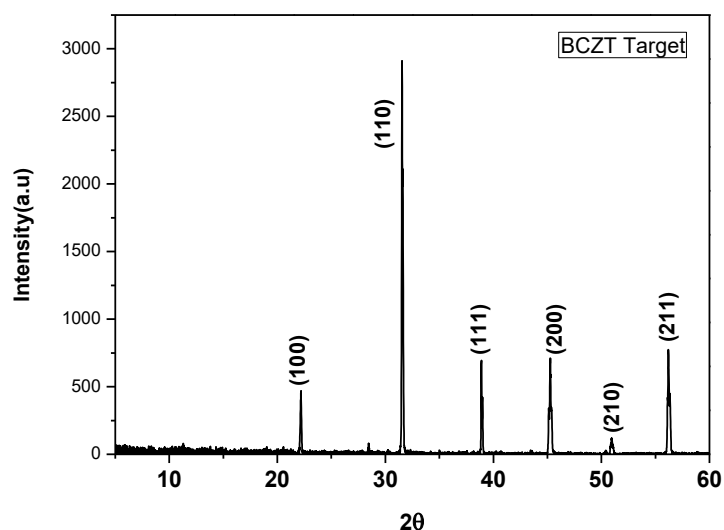


Fig5.1 Powder diffraction pattern of BCZT target

The coupled Θ - 2Θ X-Ray Diffraction of the bulk BCZT target at room temperature confirms the phase purity as shown in fig5.1. There is no impurity phase present. The (200) peaks splits into three distinguished peak which is unique for orthorhombic structures. The peak splitting is shown below in fig5.2. The lattice parameters calculated are $c=4.020\text{\AA}$, $b=4.010\text{\AA}$ and $a=4.000\text{\AA}$.

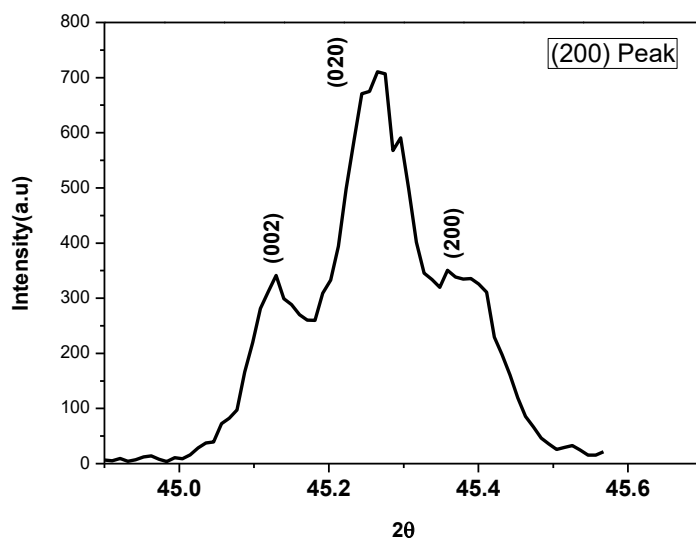


Fig5.2 BCZT peak splitting at (200) plane

BZT Target

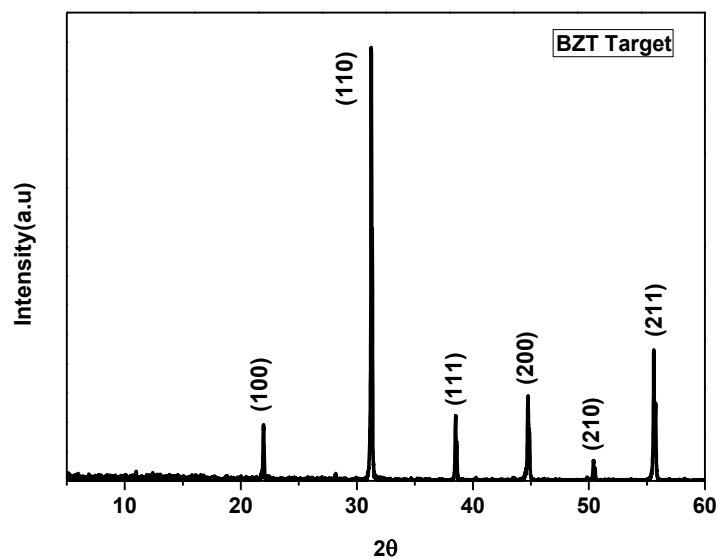


Fig5.2 Powder diffraction pattern of BZT Target

The bulk BZT Target coupled Θ - 2Θ X-Ray Diffraction at room temperature confirms the phase purity as shown in fig5.2. The peak splitting of (200) planes into doublet shows the characteristic of tetragonal crystal system. The peak splitting of (200) planes is shown below in fig5.3. The lattice parameters calculated are $c=4.044\text{\AA}$, $a=b=4.036\text{\AA}$.

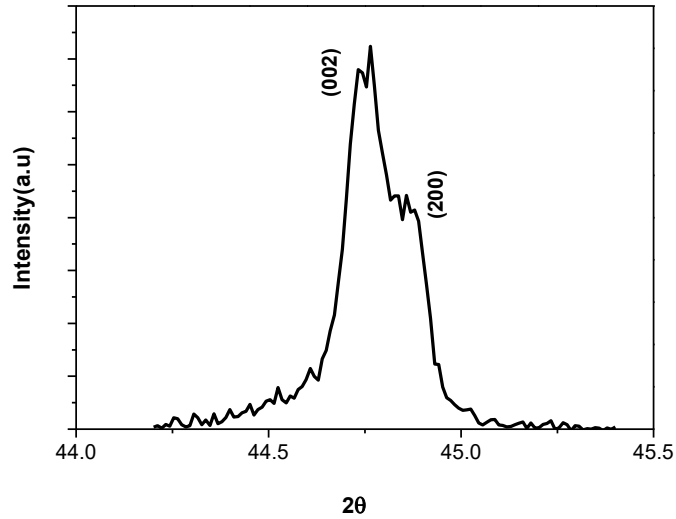


Fig5.3 Peak splitting of (200) planes

BCT Target

The bulk BCT target analysed with XRD at room temperature confirms the phase formation, however, a minor impurity phase of calcium titanate was also observed (see fig5.4). The impurity percentage was calculated to be 4%. The peak splitting of (200) planes into doublet shows the characteristic tetragonal crystal structure. The peak splitting of (200) planes is shown below in fig5.5. Calculated lattice parameters are $a=b=3.958\text{\AA}$, $c=4.000\text{\AA}$.

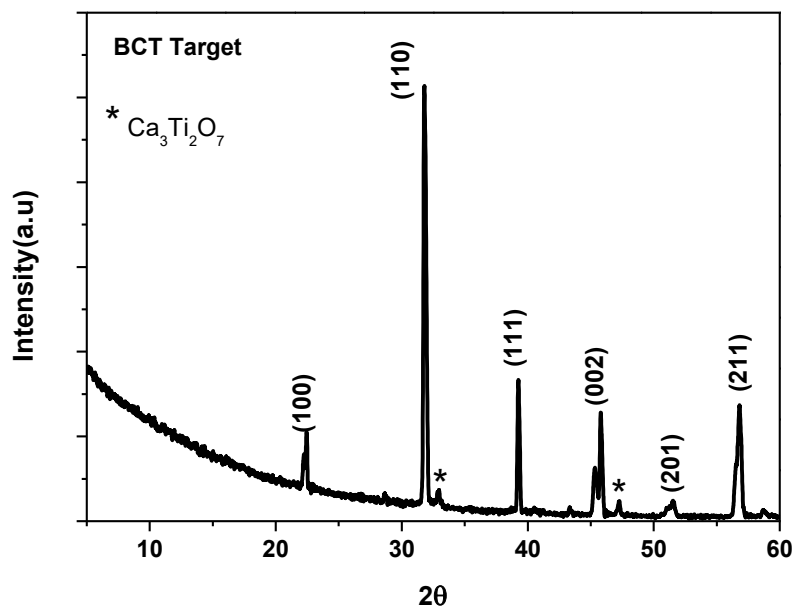


Fig5.4 Powder diffraction pattern BCT Target

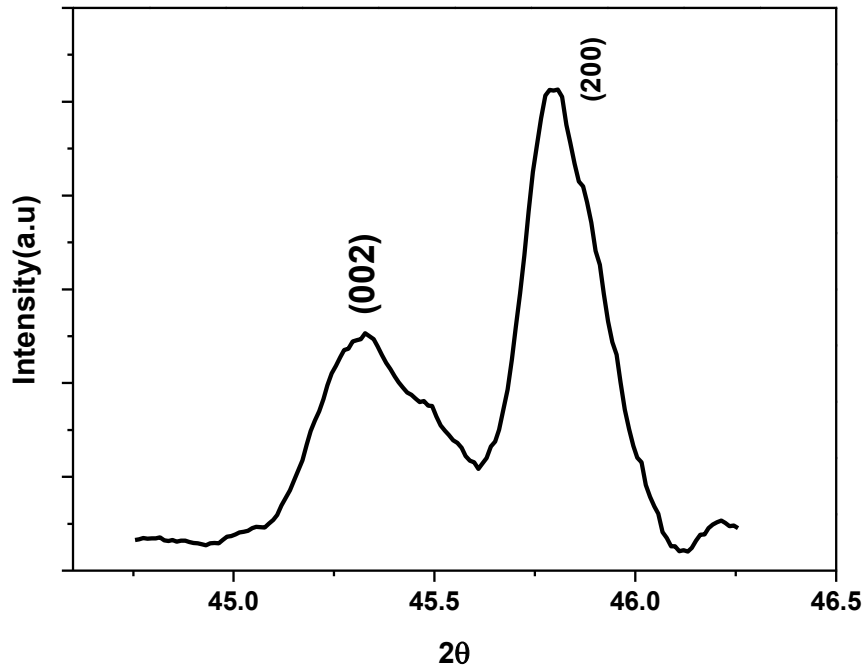


Fig5.5 BCT Tetragonal splitting at (200) planes

Deposition of thin films using pulse laser ablation technique

The sintered BCZT, BZT and BCT pellets are used as a target material in PLD to deposit polycrystalline thin film on platinum (111) coated silicon substrates. Before deposition, the substrate were heated in propanol up to 60°C for cleaning purpose. The optimized condition under which polycrystalline films are formed are shown below in Table 5.1:

Table 5.1: Table detailing the various growth parameters utilized for BCZT/BCT/BZT and bilayer using PLD

Parameters	BCZT	BZT	BCT	BCT/BZT
Base pressure (mbar)	5×10^{-5}	5×10^{-5}	5×10^{-5}	5×10^{-5}
Laser beam energy	250mJ	300mJ	300mJ	300mJ
Laser repetition rate	5Hz	5Hz	5Hz	5Hz
Oxygen pressure (mbar)	1.3×10^{-1}	1.3×10^{-1}	1.3×10^{-1}	1.3×10^{-1}
Number of pulses	6000	6000	6000	150
Substrate temperature	650°C	675°C	675°C	675°C

GIXRD of the BCZT, BZT, BCT and bilayer BCT/BZT polycrystalline films are shown below.

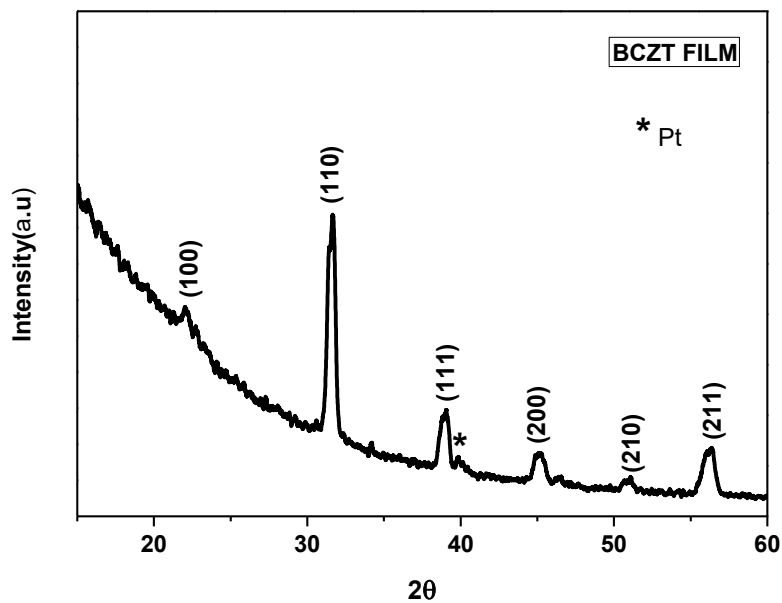


Fig5.6 Grazing incidence x ray diffraction pattern BCZT Film

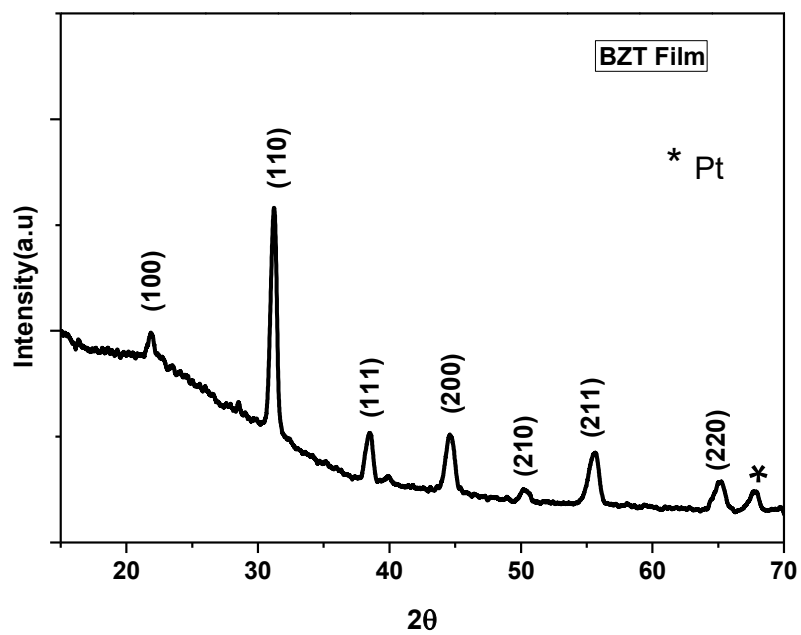


Fig5.7 Grazing incidence x ray diffraction pattern BZT Film

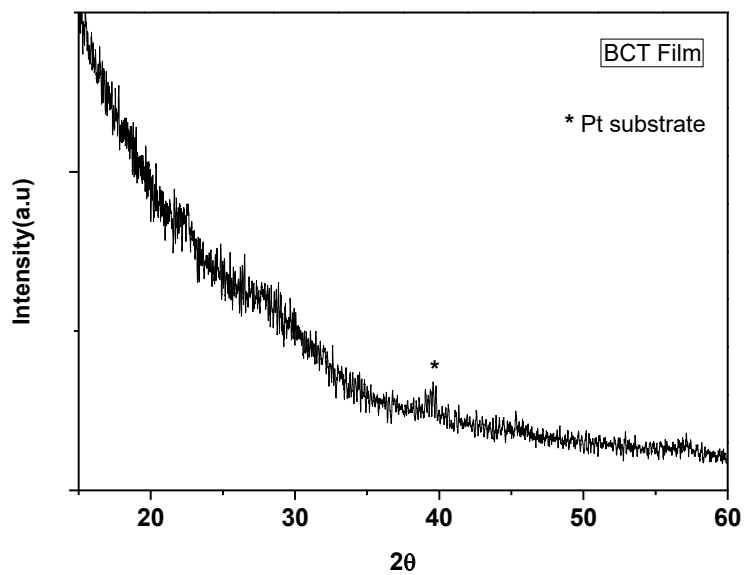


Fig5.8 Grazing incidence x ray diffraction pattern BCT Film

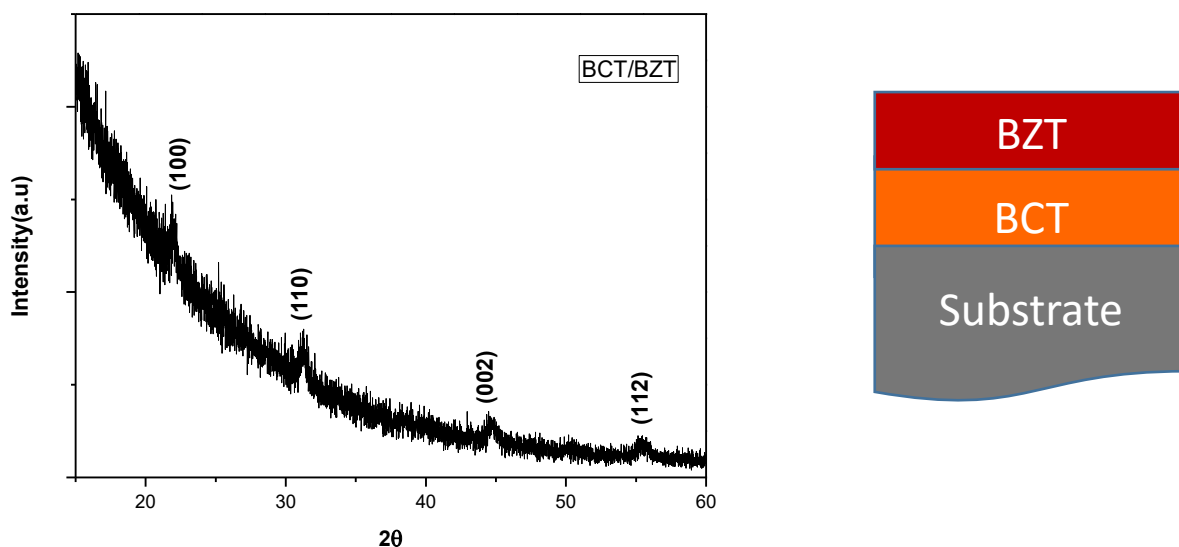


Fig5.9 Grazing incidence x ray diffraction pattern BCT/BZT Bilayer

In summary all the films grown on top of platinum coated silicon is polycrystalline in nature and there is no impurity phase present in BCZT and BZT films. The peak that appears apart from the parent phase as shown in the GIXRD plot arises from the platinum substrate. In BCT film phase formation is not so evident. BCT/BZT bilayer shows phase pure perovskite film but this can be attributed to BZT film only as phase formation of BCT film is not clear.

5.2 Surface morphological studies of thin films by using Atomic force microscopy

The surface morphology studies of the deposited thin films were done by using atomic force microscopy in tapping mode. The scan area is $4\mu\text{m}^2$. Analysis of individual films are detailed as follows:

Morphological studies

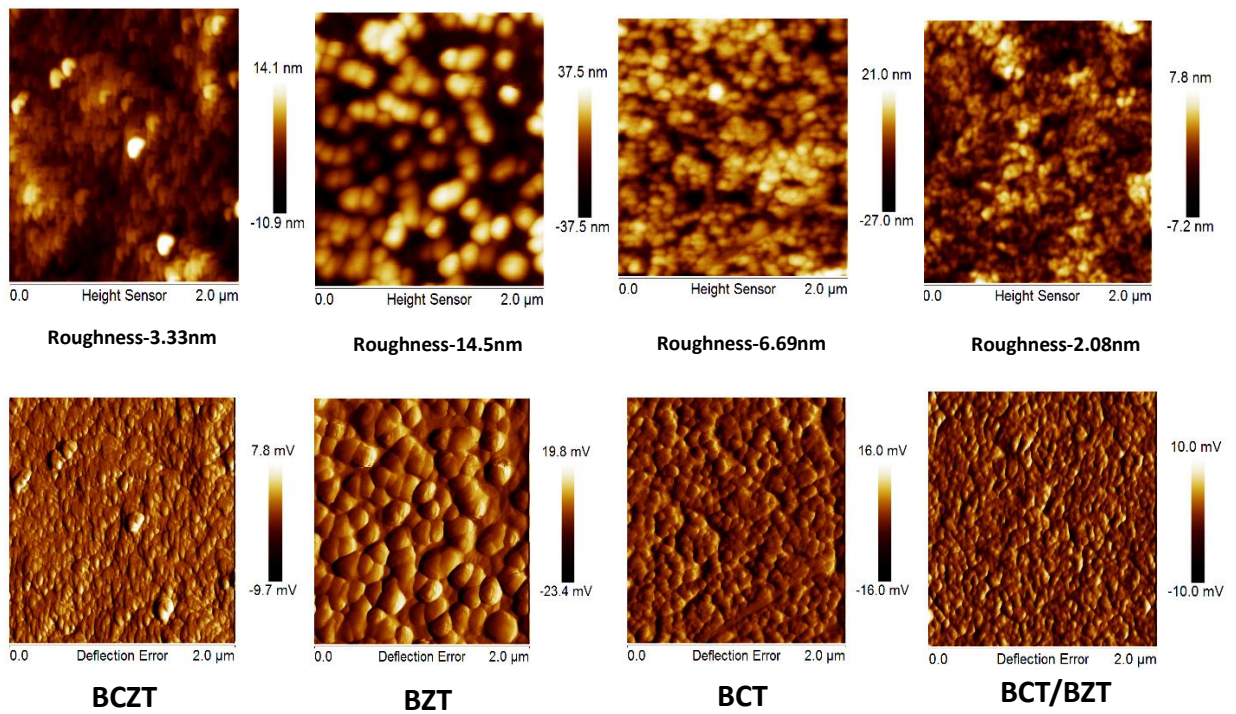


Fig5.10 AFM study of BCZT, BZT, BCT and BCT/BZT bilayer films

BCZT Film

The root mean square surface roughness of the BCZT film deposited at 675°C is around ~ 3.3 nm. Clearly some island growth could be seen in the AFM image whose size is approximately 164nm.

BZT Film

The root mean square surface roughness of the BZT film deposited at 675°C is around ~ 14.5nm. It is evident from the AFM image that the grain size is very much coarser in compare to other films. The average grain size is around 200nm.

BCT Film

The root mean square surface roughness of the BCT film deposited at 675°C is around 6.69nm. The average grain size is around 100nm.

BCT/BZT Bilayer

The root mean square surface roughness of the BCT/BZT bilayer film deposited at 675°C is around 2.08nm. The average grain size was around 80nm. There is a clear sign that in compare to BCT and BZT individual films the bilayer surface roughness had reduced and also the grain size of the BZT film which is at the top layer.

In summary BCT/BZT bilayer is having the least surface roughness of ~ 2.1nm and the highest surface roughness is of BZT film of 14.5nm. Also when BZT film is deposited on top of BCT film the surface roughness have reduced to 2.08nm and even the grain size distribution.

5.3 Piezoresponse of BCT, BZT, BCT/BZT and BCZT films

The piezoresponse force microscopy was done in contact mode. The scan area is 4 μm^2 . Analysis of individual thin film samples are detailed as follows:

BCT Film

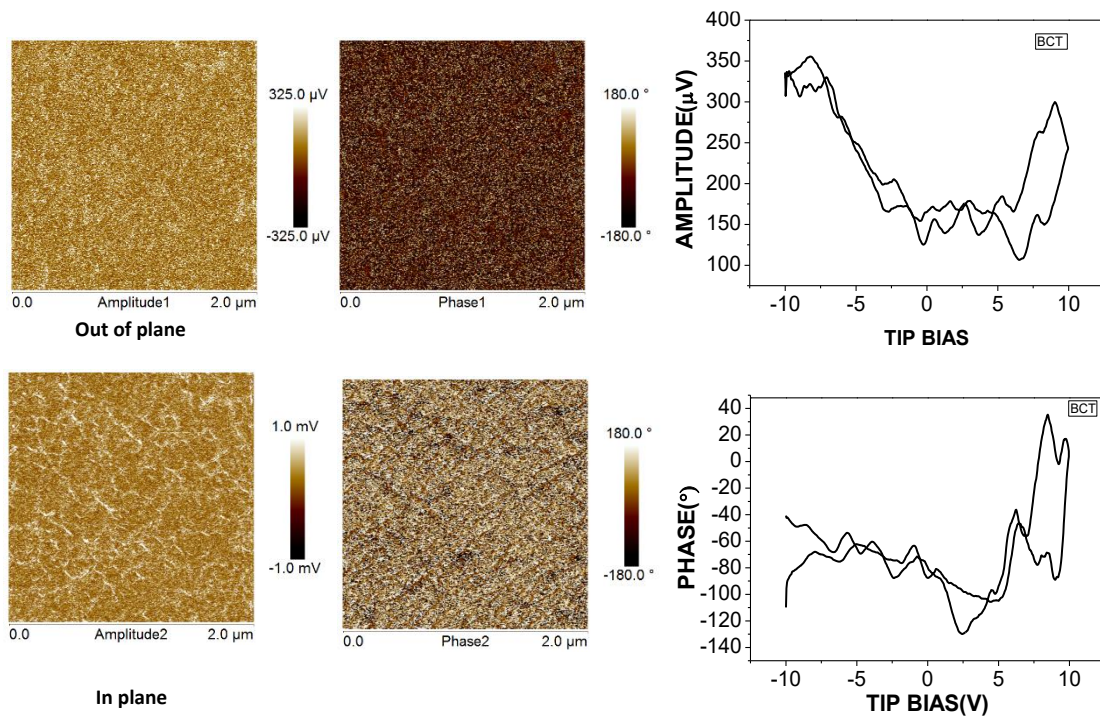


Fig5.11 Piezoresponse behavior of BCT thin film

It is clear from the PFM image there is no out-of-plane and in-plane contrast. So there is no domain formation. It is evident from the phase switching behaviour as there is no 180 degree switching and hence the film might not possess FE characteristics. The single point measurements show a noisy butterfly strain loop. Thus it can be said that in BCT thin films fabricated in this study ferroelectric behaviour is absent.

BZT Film

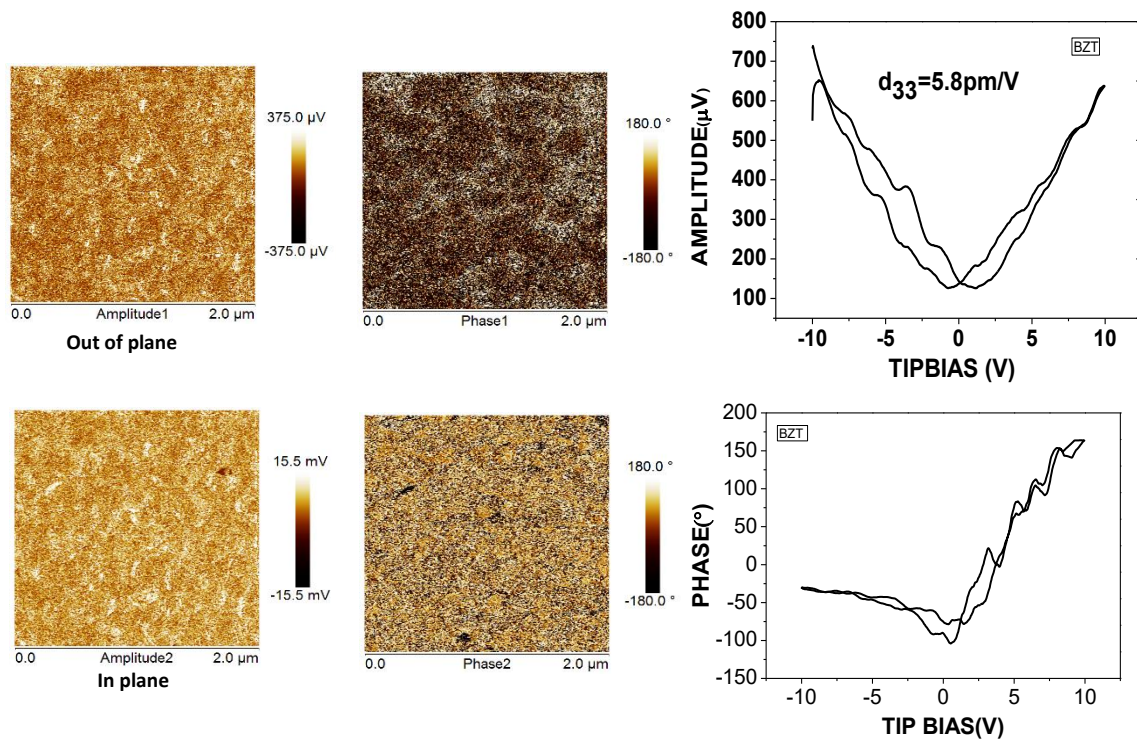


Fig5.12 Piezoresponse behavior of BZT thin film

In BZT films there is no contrast in out of plane and in plane measurement. But in single point measurements a clear butterfly loop is obtained. The phase switching behaviour of 180 degree is also evident. The d_{33} value of this BZT film is 5.8pm/V. Thus the BZT film unambiguously possess a weak ferroelectric nature.

BCT/BZT Bilayer film

In bilayer BCT/BZT film the top layer BZT film is deposited on BCT film. As PFM is a surface sensitive measurement, Piezoresponse is expected to be dominated by the BZT film. As observed it is clear from the PFM image below that it is mimicking the individual BZT film nature. There is no contrast in out-of-plane and in-plane measurement. However, a clear butterfly strain loop and feeble 180 degree phase switching is observed.

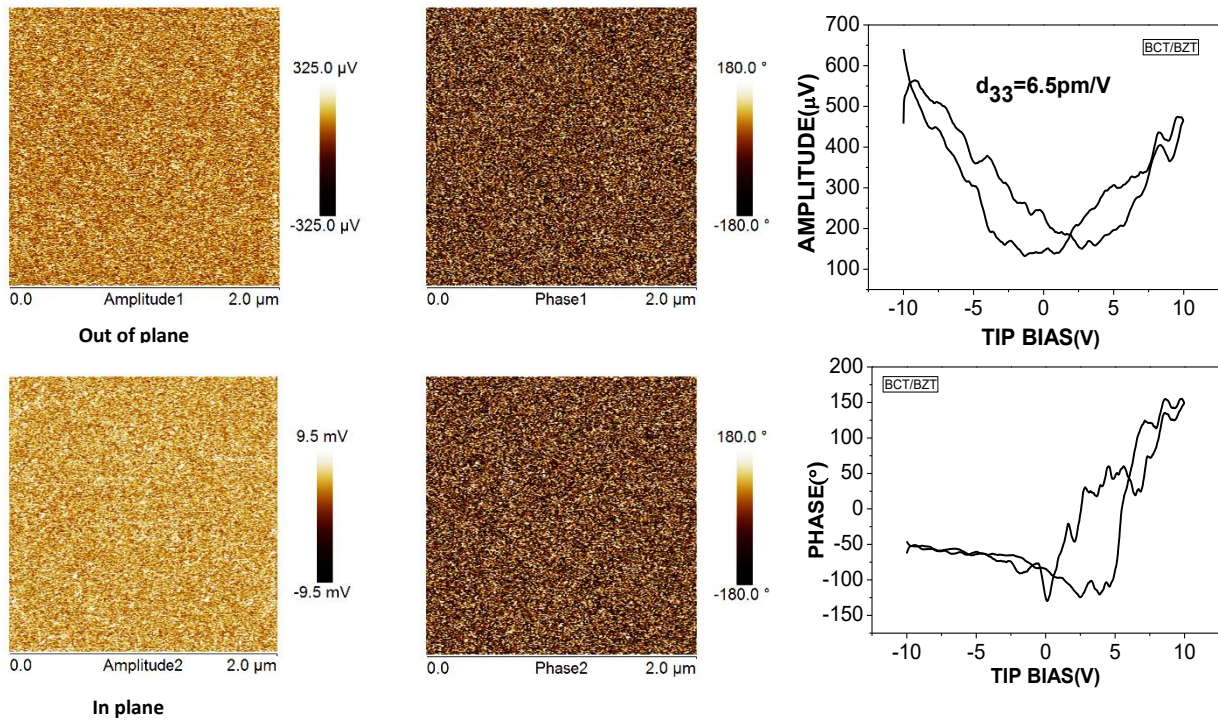


Fig5.13 Piezoresponse behavior of BCT/BZT bilayer film

Thus the bilayer BCT/BZT film is showing weak ferroelectric behaviour. The d_{33} value measured is 6.5pm/V.

BCZT Film

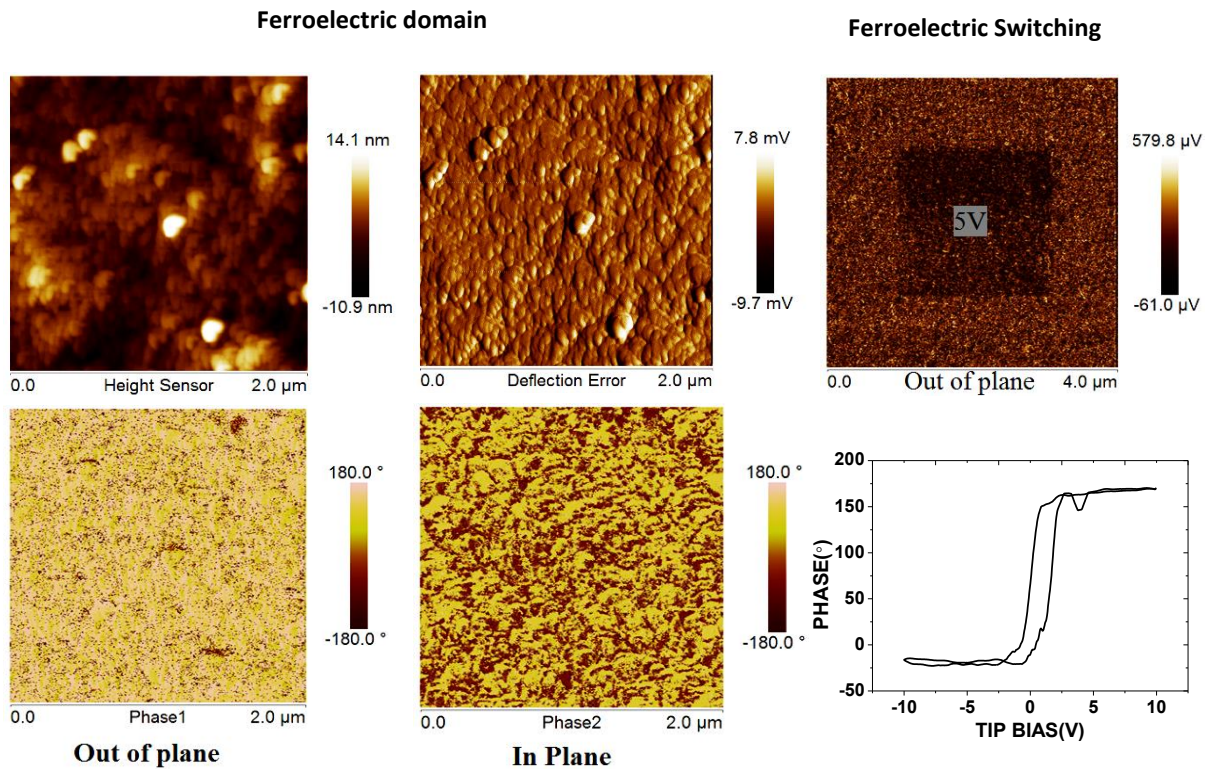


Fig5.14 Piezoresponse of BCZT thin film

In BCZT film there is a strong contrast in the in-plane measurement in compare to out-of plane. The ferroelectric domain formation is clearly evident from the in-plane response. The 180 degree phase switching is observed with saturation. This shows a strong evidence for the presence of ferroelectric nature in BCZT thin films. The measured d_{33} value of BCZT film is 20.8pm/V.

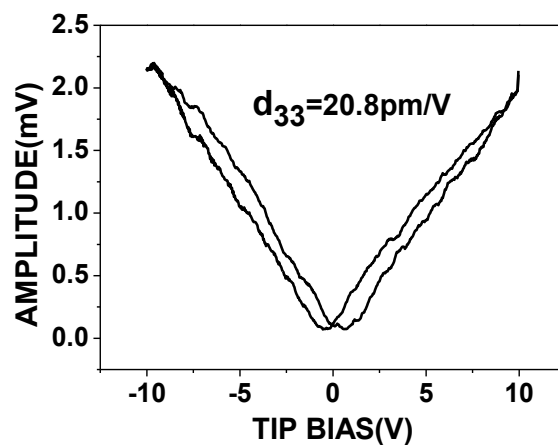


Fig5.15 Butterfly curve for BCZT thin film

5.4 V-I characterization

To study the Current-Voltage behaviour (V-I) or the leakage current all the films were fabricated in metal –insulator-metal configuration. The delay time is 0.5sec and holding time is null. The top and bottom electrodes were platinum. Circular dots of 500 μ m size were deposited on top of films by E-beam evaporation technique. As the thickness of individual films were different, the voltage was converted into Electric field. The current was converted into current density taking the diameter of the circular dots as 500 μ m. The thickness of the individual films are listed in the Table.

Table 5.2: Table detailing the thickness of BCZT/BCT/BZT and bilayer deposited using PLD

FILM	BCT	BZT	BCZT	BCT/BZT
THICKNESS	535.1nm	476.86nm	445.9nm	150nm

The Current density vs Electric field of the individual films measured are shown below:

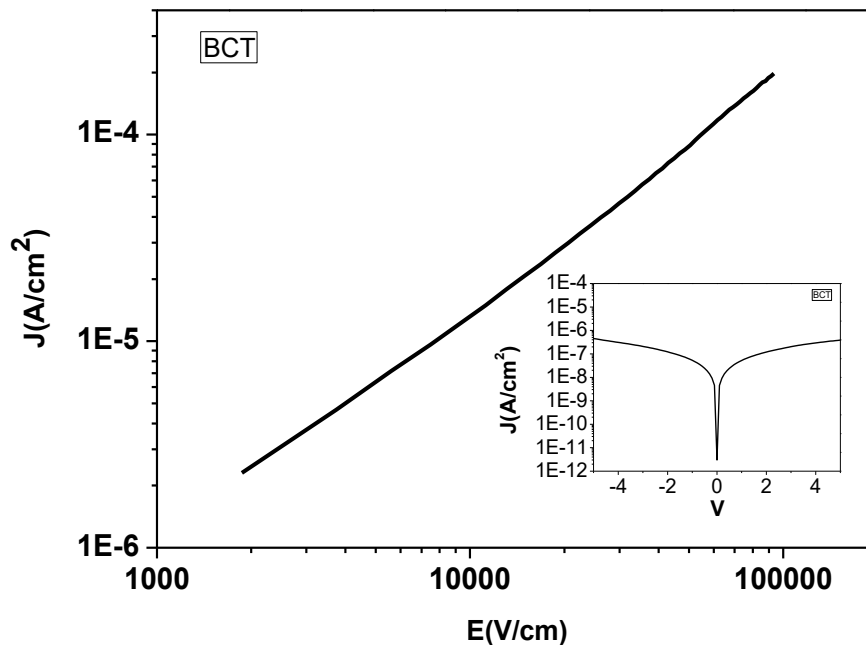


Fig5.16 Leakage current character of BCT film

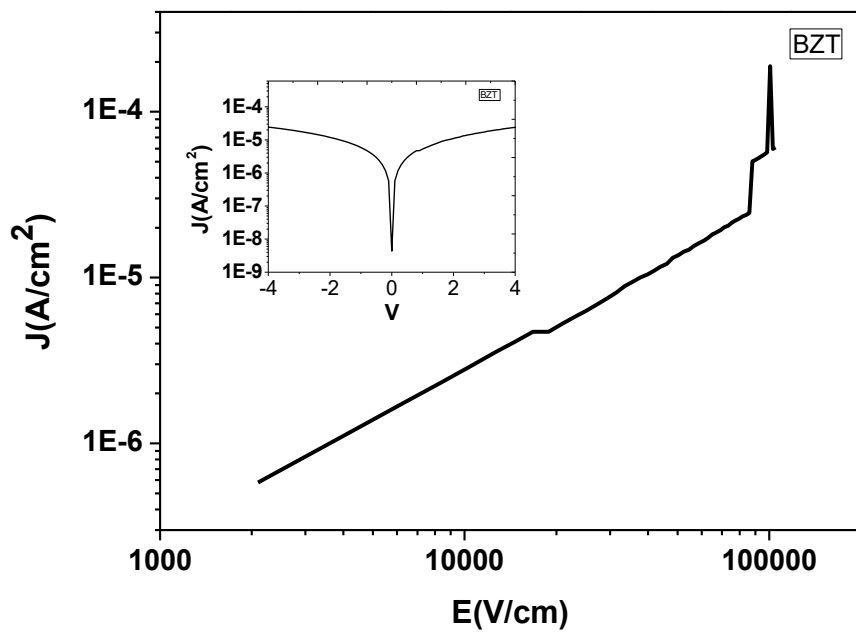


Fig5.17 Leakage current character of BCT film

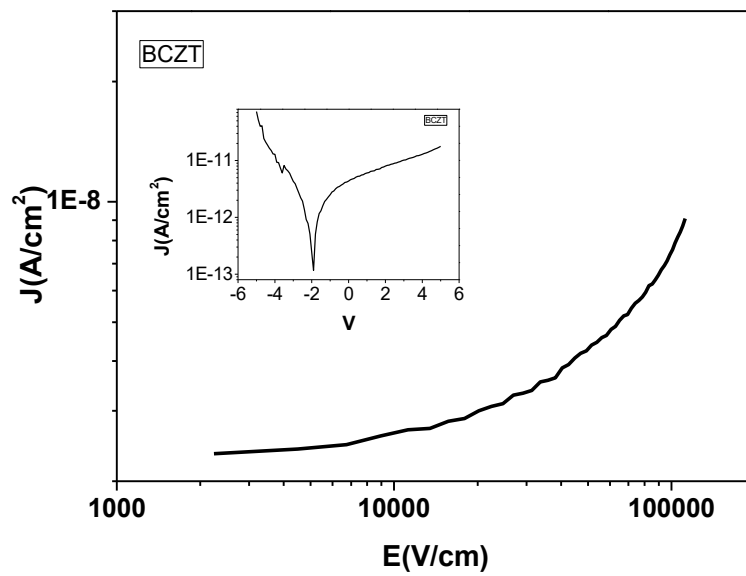


Fig5.18 Leakage current character of BCZT film

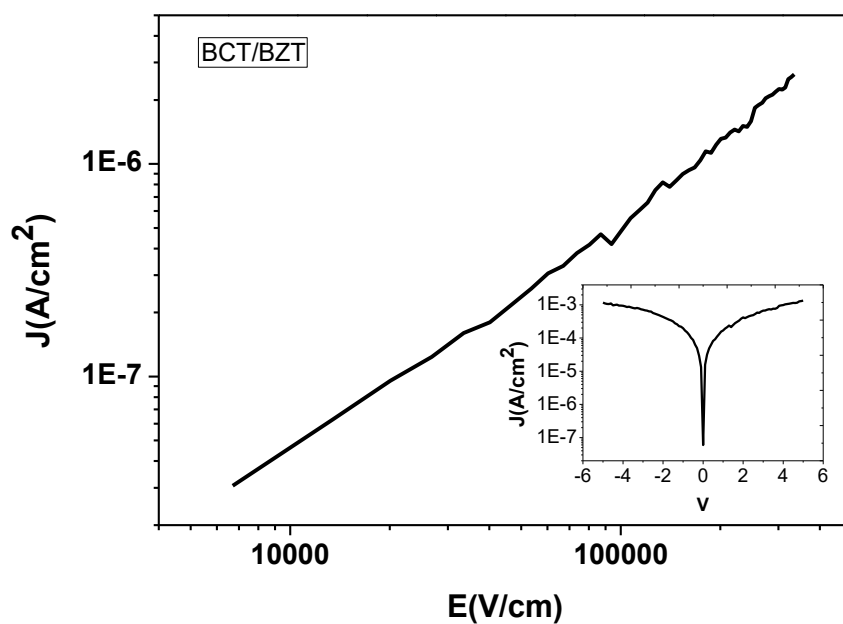


Fig5.19 Leakage current character of BCT/BZT film

5.5 Leakage current comparison

Table 5.3: Leakage current density vs electric field measurement for BCZT, BCT, BZT and bilayer films deposited using PLD

E(kV/cm)	BCT J (A/cm ²)	BZT J (A/cm ²)	BCZT J (A/cm ²)	BCT/BZT J (A/cm ²)
10	$1.31 \cdot 10^{-5}$	$2.77 \cdot 10^{-6}$	$7.4 \cdot 10^{-10}$	$4.3 \cdot 10^{-8}$
25	$3.76 \cdot 10^{-5}$	$6.27 \cdot 10^{-6}$	$1.5 \cdot 10^{-9}$	$1.15 \cdot 10^{-7}$
50	$8.78 \cdot 10^{-5}$	$1.35 \cdot 10^{-5}$	$2.86 \cdot 10^{-9}$	$2.36 \cdot 10^{-7}$
75	$1.50 \cdot 10^{-4}$	$2.12 \cdot 10^{-5}$	$3.46 \cdot 10^{-9}$	$3.87 \cdot 10^{-7}$

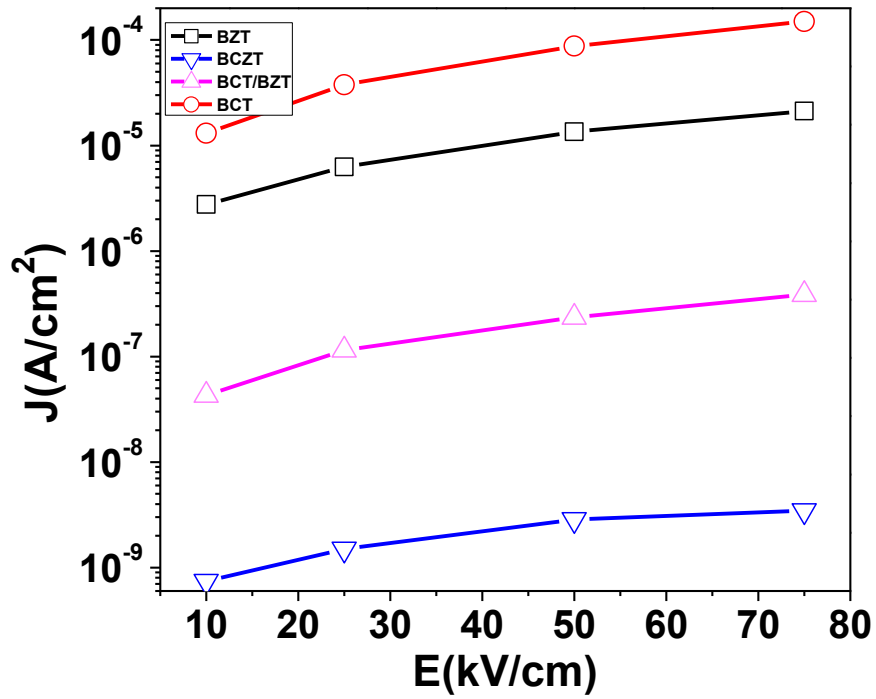


Fig5.20 Leakage current vs electric field comparison for BCT, BZT, BCZT and BCT/BZT bilayer film

The above leakage current comparison shows that the BCZT film is having the least leakage current and the leakage current value in bilayer BCT/BZT is improved in compare to its individual films.

Chapter6

Summary and conclusions

6.1 Summary

In this thesis we have synthesized three bulk BCT, BZT and BCZT targets by solid state route and fabricated thin films by optimizing the conditions to deposit polycrystalline thin films on platinum (111) coated silicon. The objective of the work was to mimic BCZT solid solution Morphotropic phase composition via multilayer approach through BCT and BZT multilayer deposition. The bulk structural characterisation was done by coupled Θ - 2Θ X Ray Diffraction and the thin films were characterised by GIXRD. The surface morphological studies were done by Atomic Force Microscopy in tapping mode and the ferroelectric nature was analysed by piezoforce microscopy in contact mode. The conclusion made are listed as below:

6.2 Conclusions:

- Phase pure BCZT and BZT targets were synthesized by solid state synthesis and polycrystalline films of their respective targets were achieved by Pulse Laser Ablation Technique.
- BCT target was synthesized with calcium titanate present as an impurity phase with 4% and film phase formation was not so evident.
- Bulk XRD analysis shows BCZT as an orthorhombic crystal structure and BCT and BZT as a tetragonal crystal system.
- The crystal structures of the thin film samples could not be verified from the powder diffraction pattern due to the weak intensity.
- Surface morphological studies shows bilayer BCT/BZT film is having the least surface roughness value of 2.08nm. Individual layers of BCT and BZT shows a surface roughness value of 6.69nm and 14.5nm which is larger than the bilayer.
- The BCZT solid solution film shows a very strong ferroelectric behaviour in comparison to other films.
- The leakage current density is minimum for BCZT solid solution film.

Future work

1. BCT polycrystalline thin film fabrication conditions need to be optimized.
2. In the grown BCT/BZT bilayer film interfacial effect of MPB composition is not so evident, so the thickness of both the films need to be optimized.
3. To achieve the piezo-coefficient value of BCZT thin film, multilayer or superlattice structure need to be fabricated.
4. Leakage conduction mechanism for all the films need to be analysed.

References

1. Devonshire, A., *Theory of ferroelectrics*. Advances in physics, 1954. **3**(10): p. 85-130.
2. <http://mentors.tanms-erc.org/mentor-responsibilities/piezoelectric-characterization>.
3. Koval, S., et al., *First-principles study of ferroelectricity and isotope effects in H-bonded K H 2 P O 4 crystals*. Physical Review B, 2005. **71**(18): p. 184102.
4. Slater, J., *The Lorentz correction in barium titanate*. Physical Review, 1950. **78**(6): p. 748.
5. <https://commons.wikimedia.org/wiki/File:Perovskite.svg>.
6. Cohen, R.E., *Origin of ferroelectricity in perovskite oxides*. Nature, 1992. **358**(6382): p. 136-138.
7. Haertling, G.H., *Ferroelectric ceramics: history and technology*. Journal of the American Ceramic Society, 1999. **82**(4): p. 797-818.
8. Cross, L.E., *Ferroelectric materials for electromechanical transducer applications*. Japanese journal of applied physics, 1995. **34**(5S): p. 2525.
9. Heywang, W., K. Lubitz, and W. Wersing, *Piezoelectricity: evolution and future of a technology*. Vol. 114. 2008: Springer Science & Business Media.
10. Liu, W. and X. Ren, *Large piezoelectric effect in Pb-free ceramics*. Physical Review Letters, 2009. **103**(25): p. 257602.
11. Kay, H.F. and P. Vousden, *XCV. Symmetry changes in barium titanate at low temperatures and their relation to its ferroelectric properties*. The London, Edinburgh, and Dublin Philosophical Magazine and Journal of Science, 1949. **40**(309): p. 1019-1040.
12. <http://what-when-how.com/electronic-properties-of-materials/electrical-properties-of-polymers-ceramics-dielectrics-and-amorphous-materials-part-3/>.
13. Fu, D. and M. Itoh, *Role of Ca off-centering in tuning the ferroelectric phase transitions in Ba (Zr, Ti) O3 system*. arXiv preprint arXiv:1503.00406, 2015.
14. <http://abulafia.mt.ic.ac.uk/shannon/radius.php?Element=Zr>.
15. Maiti, T., R. Guo, and A. Bhalla, *Evaluation of experimental resume of BaZrxTi1-xO3 with perspective to ferroelectric relaxor family: An overview*. Ferroelectrics, 2011. **425**(1): p. 4-26.
16. DeVries, R. and R. Roy, *Phase Equilibria in the System BaTiO3—CaTiO3*. Journal of the American Ceramic Society, 1955. **38**(4): p. 142-146.
17. Keeble, D.S., et al., *Revised structural phase diagram of (Ba0.7Ca0.3TiO3)-(BaZr0.2Ti0.8O3)*. Applied Physics Letters, 2013. **102**(9): p. 092903.
18. Subramanyam, G., et al., *Challenges and opportunities for multi-functional oxide thin films for voltage tunable radio frequency/microwave components*. Journal of Applied Physics, 2013. **114**(19): p. 191301.
19. <http://nptel.ac.in/courses/103103026/module2/lec12/1.html>.
20. Cullity, B.D., *Elements of X-ray Diffraction*. 2001.
21. <http://www.slideshare.net/icernatescu/gixrd>.
22. <https://en.wikibooks.org/wiki/Nanotechnology/AFM>.
23. <http://biomechanicalregulation-lab.org/afm/>.
24. Soergel, E., *Piezoresponse force microscopy (PFM)*. Journal of Physics D: Applied Physics, 2011. **44**(46): p. 464003.
25. Proksch, R. and S. Kalinin, *Piezoresponse force microscopy with asylum research AFMs*. PFM App Note, 2008.